ETHYLENE RESPONSE FACTOR 115 integrates jasmonate and cytokinin signaling machineries to repress adventitious rooting in *Arabidopsis*

Abdellah Lakehal[1], Asma Dob[1], Zahra Rahneshan [1,2,a], Ondřej Novák[3,4], Sacha Escamez[1], Sanaria Alallaq[1], Miroslav Strnad[3], Hannele Tuominen[1], Catherine Bellini [1, 5 *]

[1] Umeå Plant Science Centre, Department of Plant Physiology, Umeå University, SE-90736 Umeå, Sweden

[2] Department of Biology, Faculty of Science, Shahid Bahonar University, Kerman 76169-14111, Iran

[3] Laboratory of Growth Regulators, Faculty of Science, Palacký University and Institute of Experimental Botany, The Czech Academy of Sciences, 78371 Olomouc, Czech Republic

[4] Umeå Plant Science Centre, Department of Forest Genetics and Physiology, Swedish Agriculture University, SE-90183 Umea, Sweden

5 Institut Jean-Pierre Bourgin, INRAE, AgroParisTech, Université Paris-Saclay, FR-78000 Versailles, France

[a] Present address: Umeå Plant Science Centre, Department of Forest Genetics and Physiology, Swedish Agriculture University, SE-90183 Umea, Sweden

[*] To whom correspondence should be addressed:
Pr Catherine Bellini (catherine.bellini@umu.se /catherine.bellini@inrae.fr)
Umeå Plant Science Centre, Department of Plant Physiology,
Umeå University, SE-90736 Umeå, Sweden
Phone: +46907869624

Short title: *ERF115* controls ARI by modulating cytokinin signaling

The author responsible for distribution of materials integral to the findings presented in this article in accordance with the policy described in the Instructions for Authors (www.plantcell.org) is : Catherine Bellini (catherine.bellini@umu.se)

ABSTRACT

Jasmonate (JA), an oxylipin-derived phytohormone, plays crucial roles not only in plant immunity and defense against herbivorous insects but also in plant growth and developmental processes, including regeneration and organogenesis. However, the mechanistic basis of its mode of action and precise role in integrating other signaling cues are poorly understood. Here we provide genetic indications that JA signaling acts in both NINJA-dependent and -independent modulation of the transcriptional activity of MYC transcription factors involved in the inhibition of adventitious root initiation (ARI). Our data show that NINJA-dependent JA signaling in pericycle cells blocks early events of ARI. Moreover, transcriptomic comparison of *ninja-1myc2-322B* double mutant (which produce extremely few ARs) and wild type seedlings identified a novel molecular network governed by the APETALA2/ETHYLENE RESPONSE FACTOR 115 (ERF115) transcription factor. We demonstrate that JA-induced *ERF115* activates the cytokinin signaling machinery and thereby represses ARI. Altogether, our results reveal a molecular network involving cooperative crosstalk between JA and CK machineries that inhibits ARI.

Key words:

Jasmonate, cytokinins, adventitious rooting, AP2/ERF transcription factors, *de novo* organogenesis.

53 **INTRODUCTION**

54 Jasmonate (JA), a stress-induced phytohormone, plays crucial roles in plant immunity and
55 defense against herbivorous insects (Wasternack and Hause, 2013). It also participates in
56 control of diverse developmental processes, including tissue regeneration and rhizotaxis
57 (Wasternack and Hause, 2013; Lakehal et al., 2020). The isomer (+)-7-iso-JA-Ile (JA-Ile), the
58 bioactive form of JA (Fonseca et al., 2009), is perceived by the F-box protein CORONATINE
59 INSENSITIVE1 (COI1), which is an integral component of the Skp-Cullin-F-box (SCF)
60 complex (Xie et al., 1998). The COI1 receptor fine-tunes the function of the JA transcriptional
61 machinery in a simple manner. Briefly, in the resting state, marked by low JA-Ile contents, the
62 transcriptional activity of a number of transcription factors, including the basic-Helix-loop-
63 Helix MYC, is repressed by JASMONATE ZIM DOMAIN (JAZ) repressors through either
64 physical interaction or recruitment of the general co-repressor TOPLESS (TPL) or TPL-related
65 proteins (TPRs) (Chini et al., 2007; Thines et al., 2007; Yan et al., 2007). The adaptor NOVEL
66 INTERACTOR OF JAZ (NINJA) mediates interaction of JAZs with TPL or TRPs (Pauwels et
67 al., 2010). During activation, marked by accumulation of JA-Ile, JAZs form co-receptor
68 complexes with COI1. This interaction is facilitated by JA-Ile, which acts as a molecular glue
69 (Sheard et al., 2010). Formation of the co-receptor complexes triggers ubiquitylation and
70 proteasome-dependent degradation of the targeted JAZs, thereby releasing the transcription
71 factors to transcriptionally induce or repress their downstream target genes. Biochemical
72 studies suggest that JAZ-dependent repression machinery can inhibit the transcriptional activity
73 of different MYCs in different ways, depending on the JAZ protein involved (Chini et al.,
74 2016). However, the biological roles of this multilayered regulation are unclear, largely because
75 multiple *jaz* mutations may cause phenotypic deviations, but not single loss-of-function
76 mutations (Campos et al., 2016; Guo et al., 2018).

77 JA signaling counteracts or cooperates with a number of hormonal and signaling cascades in
78 the control of plant growth and development (Wasternack and Hause, 2013). We have
79 previously shown that the COI1-dependent MYC2-mediated JA signaling inhibited the intact
80 hypocotyl-derived ARI downstream of the auxin signaling machinery (Gutierrez et al., 2012)
81 (Figure 1). Accordingly, in contrast to the *MYC2*-overexpressing line *35S:MYC2*, the loss-of-
82 function mutant *myc2* produces more ARs than wild type plants, indicating that MYC2 plays
83 an important role in inhibition of ARI downstream of auxin (Gutierrez et al., 2012). Recently,
84 we also showed that the TIR1- and AFB2-dependent auxin signaling pathways promote ARI
85 by negatively controlling JA content (Lakehal et al., 2019a). However, despite evidence of its

central role in modulating ARI, the basis (genetic and mechanistic) and downstream targets of the MYC2-mediated JA signaling involved in this process remained unclear.

Recently, Zhou and collaborators (Zhou et al., 2019) showed that two members of subgroup X of the *APETALA2/ETHYLENE RESPONSE FACTOR (ERF)* family (*ERF109 and ERF115*) promote root stem cell niche replenishment and tissue regeneration after excision, and their expression is directly controlled by MYC2-mediated JA signaling. The *ERF115* transcription factor and its two closest homologs, *ERF114 (*also known as *ERF BUD ENHANCER* (*EBE*) and *ERF113* (also known as *RELATED to AP2.6L*, *RAP2.6L)* have been shown to control various regenerative processes, such as callus formation, tissue repair, root stem cell niche maintenance and root growth (Che et al., 2006; Nakano et al., 2006; Asahina et al., 2011; Mehrnia et al., 2013; Heyman et al., 2016; Ikeuchi et al., 2018; Kong et al., 2018; Yang et al., 2018). The three genes are rapidly induced by mechanical wounding (Ikeuchi et al., 2017), suggesting that they play an important role in connecting the stress-induced JA signaling machinery with other signaling cascades in provision of correct cell-fate and/or developmental inputs for organogenesis processes. However, how these genes coordinate and integrate the stress-induced hormonal pathways to ensure these multifunctionalities is still largely unclear. Here we provide evidence that the JA signaling machinery inhibits ARI in both NINJA-dependent and -independent manners, and the JA-induced *ERF115* transcription factor inhibits this process in a CK-dependent manner, suggesting that CKs act downstream of JA in ARI inhibition.

107 **RESULTS**

108

109 **NINJA-dependent and -independent JA signaling repress ARI**

110 To better understand the role of JA signaling during intact hypocotyl-derived ARI (Figure 1),
111 we first analyzed the AR phenotype of multiple *jaz* mutants, under previously described
112 conditions (Sorin et al., 2005; Gutierrez et al., 2009; Gutierrez et al., 2012). The quadruple loss-
113 of-function mutant *jaz7jaz8jaz10jaz13* (Thireault et al., 2015) had the same phenotype as the
114 wild type, whereas the quintuple mutant *jazQ (jaz1jaz3jaz4jaz9jaz10)* (Campos et al., 2016)
115 produced slightly fewer ARs than wild type plants (Figure 2A). These data confirm the high
116 functional redundancy of the 13 *JAZ* genes in the Arabidopsis genome (Chini et al., 2007;
117 Thines et al., 2007; Yan et al., 2007; Thireault et al., 2015; Chini et al., 2016), which
118 complicates characterization of their specificity. Therefore, we analyzed the phenotype of the
119 gain-of-function mutant *myc2-322B*, which harbors a point mutation in the transcriptional
120 activation domain (TAD) that changes Glutamate 165 to Lysine. This prevents MYC2's
121 interaction with most JAZ repressor proteins, resulting in almost constitutive MYC2 signaling
122 (Gasperini et al., 2015). We found that *myc2-322B* produced slightly fewer AR than wild type
123 plants (Figure 2B), in accordance with our previous findings that the loss-of-function mutant
124 *myc2* and overexpressing line *35S:MYC2* respectively produced more and less ARs than wild
125 type counterparts (Gutierrez et al., 2012). We also analyzed the AR phenotype associated with
126 two loss-of-function *ninja (ninja-1* and *ninja-2)* alleles (Acosta et al., 2013), because the NINJA
127 adaptor is a central hub in the transcriptional repression machinery that inactivates MYC
128 transcription factors (Pauwels et al., 2010) (Figure 1). *Ninja-1* and *ninja-2* mutants produced
129 significantly fewer ARs than wild type plants (Figure 2B), but their phenotypic deviation is
130 weak, presumably due to presence of a NINJA-independent pathway that continues to repress
131 MYCs and thus allows ARI. Because MYC2 acts additively with MYC3 and MYC4 in the
132 inhibition of ARI (Gutierrez et al., 2012), we hypothesized that removing NINJA in a *myc2-*
133 *322B* background might abolish the remaining NINJA-dependent repression and hence release
134 activity of the three MYCs. De-repression of these transcription factors would then result in
135 constitutively enhanced MYC-mediated JA signaling and block the ARI process. To test this
136 hypothesis, we analyzed the AR phenotype of two independent double mutants: *ninja-1myc2-*
137 *322B* and *ninja-2myc2-322B* (Gasperini et al., 2015). We found that ARI was almost
138 completely inhibited in both double mutants, confirming the inhibitory effect of JA (Figure 2B-
139 E). As expected, the double mutants had shorter primary roots (PRs) than wild type plants, due
140 to the inhibitory effect of JA signaling on PR growth (Staswick et al., 1992) and fewer lateral

141 roots (LRs; Supplemental Figure 1A,B), but the LR density was not affected (Figure 2C). To
142 get further genetic evidence, we also analyzed the AR phenotype of the gain-of-function mutant
143 *atr2D,* which harbors a point mutation in the JAZ interaction domain (JID) of the MYC3 protein
144 (Smolen et al., 2002) that prevents its interaction with a subset of JAZ repressors (Zhang et al.,
145 2015). Notably, there was no significant difference in AR numbers of *atr2D* mutants and wild
146 type plants, but the *ninja-1atr2D* double mutant produced far fewer ARs (Figure 2B),
147 confirming the *atr2D* mutation's additive effect and the role of MYC3 in the control of AR
148 formation. Collectively, these results genetically confirm the importance of the NINJA-
149 dependent and -independent pathways in the control of AR initiation.
150
151 ***NINJA* and *MYC2* are expressed in the etiolated hypocotyl**
152 To examine spatiotemporal expression patterns of the *NINJA* and *MYC2* genes during early
153 ARI events, we used seedlings harboring *pNINJA:GUS* or *pMYC2:GUS* transcriptional fusions
154 (Gasperini et al., 2015). The seedlings were grown in ARI-inducing conditions in the dark and
155 sampled for *pNINJA:GUS* or *pMYC2:GUS* expression analysis at T0, just before some of the
156 etiolated seedlings were exposed to light. Further samples were collected at T9L and T24L
157 (after 9 and 24 h growth in long-day conditions, respectively), while controls were sampled at
158 T9D and T24D (after a further 9 and 24 h growth in the dark, respectively). The two promoters
159 were shown to be constitutively active in all the organs at all time points, although *MYC2*
160 promoter activity declined in the cotyledons over time (Figure 3A to E). These data indicate
161 that *NINJA* and *MYC2* genes have overlapping expression domains in the hypocotyl.
162
163 **Expressing NINJA in xylem-pole pericycle cells is sufficient to counter JA's negative effect**
164 **during ARI**
165 We confirmed that the NINJA protein was broadly expressed in the hypocotyl, including the
166 xylem-pole pericycle (xpp) cells (Figure 3F) where ARs are initiated (Sorin et al., 2005;
167 Sukumar et al., 2013). We then assessed whether re-activating the NINJA-dependent JA
168 repression machinery in those cells would be sufficient to restore ARI in the *ninja1-myc2-322B*
169 double mutant. For this, we produced translational fusions of NINJA with the mCITRINE
170 reporter driven by two xpp cell-specific promoters, *GATA23* (De Rybel et al., 2010) and *XPP*
171 (Andersen et al., 2018). The p*GATA23:NINJA:mCITRINE* or p*XPP:NINJA:mCITRINE*
172 constructs were introduced into the *ninja-1myc2-322B* double mutant, and we confirmed that
173 the NINJA:mCITRINE protein was specifically present in the hypocotyl xpp cells (Figure 3G
174 and 3H). We analyzed the AR phenotype of two independent lines carrying each construct and

175 showed that in both cases the effect of the *ninja-1* mutation was complemented (Figure 3I).
176 These results suggest that expressing NINJA in xpp cells is sufficient to de-repress ARI, and
177 that NINJA-dependent JA signaling acts in early stages of ARI.
178
179 **Transcriptomic insights into JA's role in ARI**
180 To get mechanistic insights into how JA signaling reprograms the transcriptional machinery
181 during ARI, we compared transcriptomes of *ninja-1myc2-322B* double mutant and wild-type
182 hypocotyls at three time points: T0, T9 and T24 (Figure 4A). In T0 samples we detected 530
183 differentially expressed genes (DEGs), of which 462 were upregulated and 68 downregulated
184 in the *ninja-1myc2-322B* double mutant. We detected 671 DEGs at T9, 453 upregulated and
185 218 downregulated, and 579 at T24, 388 upregulated and 191 downregulated (Figure 4B,
186 Supplemental Figure 2 and Supplemental Table 1).
187
188 **The *ninja-1myc2-322B* double mutant has a constitutive JA response signature**
189 MYC transcription factors recognize and bind to hexameric *cis*-regulatory G-box motifs
190 (CACGTG or CACATG), and MYC2 binds to G box-like motifs (AACGTG, CATGTG,
191 CACGAG, CACATG, CACGCG) with differing affinities (Godoy et al., 2011). To get an
192 overview of possible direct targets of MYCs among the DEGs, we searched for these motifs in
193 the 1 kb regions upstream of their ATG translation start codons. We found that DEGs'
194 promoters are highly enriched with MYC binding sites, suggesting that they include potential
195 direct targets of MYC. At T0, T9 and T24, 64% of 520 DEGs (342: 334 upregulated and 8
196 downregulated), 62% of 671 DEGs (420: 341 upregulated and 79 downregulated), and 67% of
197 579 DEGs (389: 287 upregulated and 102 downregulated) respectively contained at least one
198 of the six motifs (Figure 4C).
199 Most of the *JAZ* genes, which are early JA-responsive genes, were highly upregulated in the
200 *ninja-1myc2-322B* double mutant at all sampling time points (Figure 4D), confirming the
201 presence of enhanced, constitutive JA signaling. Accordingly, several genes involved in JA
202 biosynthesis, such as *LIPOXYGENASE 2 (LOX2), ALLENE OXIDE SYNTHASE (AOS),*
203 *ALLENE OXIDE CYCLASE1 (AOC1), AOC3, AOC4, OXOPHYTODIENOATE-*
204 *REDUCTASE3 (OPR3) and OPC-8:0 COA LIGASE1 (OPCL1)* were upregulated in the double
205 mutant *ninja-1myc2-322B* (Figure 4E). The biological relevance of this upregulation of gene
206 expression was confirmed by findings that levels of the JA precursor *cis*-12-oxo-phytodienoic
207 acid (*cis*-OPDA), JA and JA-Ile were higher in the double mutant than in wild-type controls at
208 all time points, except that JA-Ile contents did not significantly differ at T0 (Figure 4F-H).

209 These data highlight a feedforward loop that amplifies the response to JA signaling by
210 enhancing JA biosynthesis.
211
212 **JA signaling controls expression of *ERF113*, *ERF114* and *ERF115* transcription factors.**
213 The candidate transcription factor potentiel targets of MYC2 we detected included three closely
214 related members of subgroup X of the *ERF* family (*ERF113*, *ERF114* and *ERF115*) (Figure
215 5A,B). Analysis by qRT-PCR confirmed that these three genes were all upregulated in the
216 hypocotyl of the *ninja-1myc2-322B* double mutant, except *ERF113* at T0 (Figure 5C). These
217 genes have known involvement in a number of organogenesis and regeneration processes
218 (Heyman et al., 2018). To address their role in ARI, we analyzed the AR phenotypes of
219 available single loss of *ERF113* or *ERF115* function mutants (*rap2.6l-1* and *erf115,*
220 respectively*)* and observed no significant difference in this respect between them and wild-type
221 controls (Figure 6A). As no loss-of-function T-DNA line for *ERF114* was available, we used
222 CRISPR-Cas9 technology to delete a ca. 40 bp genomic fragment in the first exon of the
223 *ERF114* gene in the *rap2.6l-1* and the *erf115* backgrounds to obtain *rap2.6l-1erf114C* and
224 *erf115erf114C* double mutants, respectively (Supplemental Figure 3). Other multiple mutants
225 were obtained by genetic crosses. Only the triple mutant *rap2.6l-1erf114Cerf115* produced
226 significantly more ARs than wild-type controls (Figure 6A), indicating that *ERF113, ERF114*
227 and *ERF115* act redundantly in the control of ARI.
228
229 ***ERF115* represses hypocotyl-derived AR initiation downstream of auxin**
230 Previous findings that *ERF115*'s expression is directly controlled by MYC2 and it plays major
231 roles in root regeneration and stem cell replenishment (Heyman et al., 2013; Heyman et al.,
232 2016; Zhou et al., 2019) prompted us to address its function during ARI. First, to overcome
233 potential functional redundancy with other members of the family, we analyzed the
234 *pERF115:ERF115:SRDX* line, which expresses a dominant negative variant of ERF115
235 (because the *ERF115* coding sequence fused to the ethylene-responsive element binding factor-
236 associated amphiphilic repression (EAR) domain is driven by the *ERF115* promoter to ensure
237 repression in the native expression domain (Heyman et al., 2013). The
238 *pERF115:ERF115:SRDX* line produced significantly more ARs than wild-type controls, but
239 was very similar to the *rap2.6l-1erf114Cerf115* triple mutant (Figure 6A,B). Although we
240 cannot exclude a potential contribution of other *ERF* genes, these findings suggest that *ERF113*,
241 *ERF114* and *ERF115* are the main transcription factors involved in ARI. Interestingly, the
242 overexpressing line *35S:ERF115* developed extremely few ARs (Figure 6B) but had only

243 slightly lower LR density than wild-type plants (Figure 6C and Supplemental Figure 4C,D).
244 Thus, it phenocopied the *ninja-1myc2-322B* double mutant and confirmed that *ERF115* is an
245 ARI repressor. We also characterized *ERF115*'s expression pattern during early ARI events
246 using lines harboring the transcriptional fusion *pERF115:GUS*(Heyman et al., 2013). At T0,
247 GUS staining was mainly detected in vascular tissues of the hypocotyl, and to a lesser extent in
248 the root (Figure 6D). Exposing the seedlings to light for 24 h dramatically decreased the GUS
249 signal (Figure 6D), suggesting that the *ERF115* gene is expressed in vascular tissue and its
250 expression is negatively regulated by light, which we confirmed by qRT-PCR (Figure 6E).
251 As JA acts downstream of auxin signaling in ARI inhibition (Gutierrez et al., 2012; Lakehal et
252 al., 2019a), we hypothesized that the *35S:ERF115* line could be insensitive to exogenously
253 applied auxin. To test this hypothesis, we treated *35S:ERF115*-expressing and wild-type pre-
254 etiolated seedlings with the synthetic auxin naphthaleneacetic acid (NAA), and found that 1
255 μM NAA significantly enhanced AR development in the wild-type seedlings, but did not affect
256 the *35S:ERF115*-expressing seedlings (Figure 6I-K). These data suggest that auxin cannot
257 bypass the inhibitory effect of *ERF115* during ARI. Notably, the PR and LRs of the
258 *35S:ERF115*-expressing seedlings were as sensitive as the wild-type roots to NAA (Figure
259 6I,J). These data suggest that *ERF115* specifically activates and/or cooperates with other
260 negative regulator(s) of ARI downstream of auxin signaling.
261
262 ***ERF115*-mediated ARI repression requires cytokinins (CKs)**
263 CKs, in balance with auxin, are known to promote shoot and callus formation but inhibit root
264 growth and AR formation (Lakehal and Bellini, 2018; Ikeuchi et al., 2019), raising the
265 possibility that modulation of the CK machinery by *ERF115* is involved in this
266 multifunctionality. We confirmed the negative role of CKs in control of ARI as exogenously
267 applied 6-benzyladenine (6-BA) inhibited the process in a dose-dependent manner (Figure 7A).
268 We then analyzed the CK-deficient triple loss-of-function mutant *ipt3ipt5ipt7* that lacks three
269 important ATP/ADP ISOPENTENYLTRANSFERASES catalyzing a rate-limiting step in *de*
270 *novo* CK biosynthesis (Miyawaki et al., 2006), and a line overexpressing *CYOKININ*
271 *OXIDASE1* (*35S:CKX1)*, which is also deficient in CKs due to their enhanced
272 degradation(Werner et al., 2003). Notably, both the triple loss-of-function mutant *ipt3ipt5ipt7*
273 and the *35S:CKX1*-expressing line produced significantly more ARs than wild-type controls
274 (Figure 7B,C). Similarly, the *arr1-3arr11-2* double mutant and *arr1-3arr11-2arr12-1* triple
275 mutant, which lack the key type-B transcription factors ARR1, ARR11 and ARR12 involved

276 in CK signaling, produced significantly more ARs than wild-type plants (Figure 7D). These
277 data genetically confirmed that CKs are repressors of ARI.
278 To test the hypothesis that *ERF115* inhibits ARI through CKs, we quantified relative amounts
279 of transcripts of two CK-responsive genes, *ARR5* and *ARR7*, in etiolated hypocotyls of the
280 overexpressing line *35S:ERF115* and wild-type controls at T0 and T24. Interestingly, at T0
281 *ARR7* was upregulated, and at T24 both *ARR5* and *ARR7* were upregulated in the *35S:ERF115*
282 line (Figure 7E). These findings suggest that CK responses are enhanced in hypocotyls of
283 *35S:ERF115* plants, and to explore possible causes we quantified active CK bases at T0, T9
284 and T24. At T0, isopentyladenine (iP), *trans*-Zeatin (*t*Z) and *cis*-Zeatin (*c*Z) contents of
285 *35S:ERF115* and wild-type plants did not significantly differ (Figure 7F). However, at T9,
286 *35S:ERF115* plants had significantly higher iP, *t*Z and *c*Z contents, and at T24 significantly
287 higher iP and *c*Z contents than wild-type controls (Figure 7F). These data suggest that the
288 *ERF115* inhibits ARI by modulating the CK pool. To test this hypothesis, we generated a
289 *35S:ERF115ipt3ipt5ipt7* multiple mutant and a line overexpressing both *35S:ERF115* and
290 *35S:CKX1* to deplete the CK pool in a *35S:ERF115* background, and confirmed that this was
291 sufficient to restore ARI to wild-type levels in the *35S:ERF115* line (Figure 7G). These data
292 indicate that *ERF115* inhibition of ARI is mediated by CKs. Interestingly, our transcriptomic
293 data showed that several *LONELY GUY* (*LOG*) genes, which control a rate-limiting step in CK
294 biosynthesis (Kuroha et al., 2009), were slightly upregulated, while several *CKX* genes were
295 slightly downregulated, in the *ninja-1myc2-322B* double mutant (Supplemental Figure 5A,B).
296 Altogether, our results strongly suggest that JA inhibits ARI by modulating CK homeostasis
297 through the action of *ERF115*
298

299 **DISCUSSION**

300 Plants develop ARs in response to diverse intrinsic and/or extrinsic (stress-induced) cues
301 (Bellini et al., 2014; Steffens and Rasmussen, 2016) that are perceived by competent cells and
302 trigger extensive reprogramming that results in targeted cells acquiring new identities (Bellini
303 et al., 2014; Lakehal and Bellini, 2018). The process has both high fundamental interest and
304 practical importance as adventitious rooting is often a limiting step in clonal propagation.
305 However, very little is known about the mechanism triggering the cell reprogramming that leads
306 to ARI. Fortunately, intact hypocotyl-derived AR provide ideal model systems to unravel the
307 signaling networks involved in this and other *de novo* organogenesis processes. We have
308 previously shown that auxin controls ARI in Arabidopsis hypocotyls by modulating JA
309 homeostasis (Gutierrez et al., 2009; Gutierrez et al., 2012; Lakehal et al., 2019a), but the JA
310 signaling mechanism involved was not clear. Here, we provide detailed genetic and mechanistic
311 insights into the JA signaling involved in ARI. Notably, *ninja-1* and *ninja-2* loss-of-function
312 mutants produce ARs, albeit fewer than wild-type controls, and several lines of evidence
313 indicate that this is possibly due to NINJA-independent repression of MYC-dependent
314 machinery by a subset of JAZ proteins. For example, JAZ5, JAZ6, JAZ7 and JAZ8 can directly
315 recruit TPL through their EAR motifs independently of NINJA (Kagale et al., 2010; Causier et
316 al., 2012; Shyu et al., 2012), while JAZ1, JAZ3 and JAZ9 can directly recruit HISTONE
317 DEACETYLASE6 (HDA6) (Zhu et al., 2011), which participates in repression of various JA-
318 induced genes' expression (Zhu et al., 2011). In addition, yeast two-hybrid experiments have
319 shown that JAZ7, JAZ8 and JAZ13 do not interact with NINJA (Pauwels et al., 2010; Shyu et
320 al., 2012; Thireault et al., 2015), and the Jasmonate-associated (Jas) domain of JAZ directly
321 binds to the region containing the JAZ-interaction domain (JID) and TAD domains of MYC2,
322 MYC3 or MYC4 (Zhang et al., 2015). Moreover, MED25 (one of 29 subunits of the
323 MEDIATOR complex) interacts with MYC proteins and recruits the RNA polymerase II-
324 dependent transcriptional machinery at MYC-target genes (Chen et al., 2012; An et al., 2017).
325 MED25 directly interacts with the TAD domain of MYCs, raising the possibly that it competes
326 with JAZ proteins for access to the TAD domain(Zhang et al., 2015). All these findings suggest
327 that some JAZ proteins might block transcriptional activities of MYC transcription factors
328 involved in ARI in a NINJA-independent manner. Further research is needed to decipher the
329 JAZ-dependent JA perception machinery involved in ARI. For this, combining mutants with
330 potentially complementary functionalities, and/or potentially informative expression patterns,
331 may be more illuminating than generating higher-order multiple mutants based on phylogenetic
332 relationships.

333

334 Our results indicate that MYC-mediated JA signaling inhibits ARI in both NINJA-dependent
335 and -independent manners. Both pathways act synergistically in control of the JA response, as
336 indicated by the much lower numbers of ARs produced by *ninjamyc2-322B* double mutants
337 than the parental lines (*ninja* and *myc2-322B*) and wild-type controls. Therefore, the strong
338 phenotype of *ninjamyc2-322B* double mutants may be due to de-repression of not only MYC2,
339 MYC3 and MYC4, but also other NINJA-bound transcription factors (if any). Interestingly,
340 this de-repression results in constitutively enhanced JA signaling. Accordingly, our
341 transcriptomic analysis revealed that most of the JAZ genes, which are JA response marker
342 genes (Chini et al., 2007), were highly and constitutively upregulated in *ninja-1myc2-322B*
343 plants throughout the covered developmental stages. Our results are consistent with previous
344 report suggesting that MYC2 controls root expansion in NINJA dependent and -independent
345 manners (Gasperini et al., 2015).
346 For many years JA was regarded as a solely stress-related plant hormone, but more recently
347 JA signaling has been implicated in several organogenesis and regenerative processes (Asahina
348 et al., 2011; Gutierrez et al., 2012; Lakehal et al., 2019a; Zhang et al., 2019; Zhou et al., 2019),
349 and attempts to identify its downstream targets have begun. Although its role in adventitious
350 rooting seems to be species- and context-dependent (Lakehal and Bellini, 2018), our results
351 indicate that the *ERF115* gene is likely one of the targets acting downstream of JA in this
352 process. This conclusion is strongly supported by the recent finding that MYC2 induces
353 expression of *ERF115* by directly binding its promoter (Zhou et al., 2019). The *ERF115* acts
354 redundantly with its closely-related paralogs *ERF113* and *ERF114,* which have also been
355 implicated in several organogenesis and regenerative processes (Heyman et al., 2018). Here we
356 provide evidence that *ERF115*-mediated ARI inhibition involves modulation of the CK
357 machinery. Physiological approaches have shown that CKs inhibit ARI in several plant species
358 and model systems (Lakehal and Bellini, 2018). In this study, we genetically demonstrated that
359 depleting CKs by either blocking their biosynthesis or enhancing their degradation restores the
360 ARI wild-type phenotype in an *ERF115*-overexpressing line, confirming that *ERF115* represses
361 ARI through CK signaling. Interestingly, the *ERF115* promoter contains a cytokinin-responsive
362 motif, and a yeast one-hybrid screen has shown that ARR1 and ARR20 bind to the promoter of
363 *ERF115* (Ikeuchi et al., 2018). Although direct evidence is needed, these data suggest that
364 cytokinin signaling may also control the abundance of *ERF115* transcripts. The role of this
365 feedback loop in adventitious rooting, if any, awaits further investigation.

366 **MATERIALS AND METHODS**

367

368 **Plant material**

369 The quadruple mutant *jaz7jaz8jaz10jaz13* (Thireault et al., 2015) and quintuple mutant
370 *jaz1jaz3jaz4jaz9jaz10*(Campos et al., 2016) were provided by G. Howe (Michigan State
371 University, USA). The single mutants *ninja-1*, *ninja-2* (Acosta et al., 2013), and *myc2-322B* as
372 well as the double mutants *ninja-1myc2-322B*, *ninja-2myc2-322B* and *ninja-1atr2D* (Gasperini
373 et al., 2015) were provided by E.E. Farmer (University of Lausanne, Switzerland). The gain of
374 function allele of *MYC3* (*atr2D*) (Smolen et al., 2002) was provided by J. Bender (Brown
375 University, Rhode Island, USA). The single mutant *erf115* (SALK_021981) and transgenic
376 lines *pERF115:ERF115:SRDX*, and *35S:ERF115* (Heyman et al., 2013) were provided by L.
377 De Veylder (VIB, University of Gent, Belgium). The *rap2-6l-1* mutant (SALK_051006) (Che
378 et al., 2006), *arr1-3arr11-2* (N6980) and *arr1-3arr11-2 arr12-1* (N6986) were provided by the
379 Nottingham Arabidopsis Stock Centre. The transgenic line *35S:CKX1* (Werner et al., 2003) and
380 triple mutant *ipt3ipt5ipt7* (Miyawaki et al., 2006) were provided by T. Schmülling (Freie
381 Universität Berlin, Germany). E.E. Farmer and L. De Veylder also respectively provided the
382 reporter lines *pMYC2:GUSplus*, *pNINJA:GUSplus* and *pNINJA:NINJA:mCITRINE/ninja-1*
383 (Gasperini et al., 2015) and *pERF115:GUS* (Heyman et al., 2013).

384

385 **CRISPR-Cas9 cloning, transformation and mutant screening**

386 To generate the loss-of-function allele *erf114*C, two guide RNAs (ERF114_F and ERF114_R,
387 see Supplemental Table 2) were designed, as previously described (Lakehal et al., 2019b), to
388 target the *ERF114* gene's first exon (Supplemental Figure 3). The guide RNAs were then cloned
389 into the binary vector pHEE401E, the resulting construct was transformed into *Escherichia coli*
390 cells, and the positive clones were selected by PCR, then confirmed by sequencing, following
391 previous protocols (Xing et al., 2014; Wang et al., 2015). The *Agrobacterium*-mediated floral
392 dip method (Clough and Bent, 1998) was used to transform the construct into *rap2-6l-1* or
393 *erf115* mutants. T1 seedlings were screened on Arabidopsis growth medium (Lakehal et al.,
394 2019b) containing 50 µg/ml hygromycin and surviving seedlings were genotyped for deletions
395 in *ERF114* using primers listed in Supplemental Table 2. Several independent homozygous and
396 heterozygous T1 lines were identified. Only homozygous *erf114C* and Cas9-free lines,
397 confirmed by examination of T2 individuals and Cas9-construct genotyping (Xing et al., 2014;
398 Wang et al., 2015), were used for further analysis.

399

400

401 **Tissue-specific complementation: cloning, transformation and transgenic line screening**

402 The pEN-L4-pGATA23-R1 and pEN-L4-pXPP-R1 plasmids (De Rybel et al., 2010) (Andersen
403 et al., 2018) were gifts from T. Beeckman (VIB, Gent, Belgium) and J. Vermeer (University of
404 Zurich, Switzerland), respectively. Plasmids carrying coding sequences of the *NINJA* gene,
405 pEN-L1-NINJA(noSTOP)-L2, and reporter protein, pEN-R2-mCITRINE-L3 (Gasperini et al.,
406 2015), were gifts from E.E. Framer (University of Lausanne, Switzerland). To generate
407 promoter:NINJA:CT fusion protein constructs, the pEN-L4-promoter-R1, pEN-L1-
408 NINJA(noSTOP)-L2 and pEN-R2-mCITRINE-L3 were recombined into the pB7m34gw
409 vector using LR clonaseII plus (Invitrogen) according to the manufacturer's instructions. All
410 the expression vectors were confirmed by colony PCR and sequencing, then transformed into
411 GV3101 *Agrobacterium tumefaciens* cells, which were used to transform *ninja-1myc2-332B*
412 double mutants using the floral dip method (Clough and Bent, 1998). Single-copy, homozygous
413 lines were selected by cultivating representatives of T2 and T3 generations on Arabidopsis
414 medium (Lakehal et al., 2019b) supplemented with 10 µg/ml DL-phosphinothricin (Duchefa
415 biochemie). At least two lines carrying each construct showing the same phenotype were further
416 characterised.

417

418 **Growth conditions and root (adventitious and lateral) phenotyping**

419 Previously described adventitious rooting conditions (Sorin et al., 2005; Gutierrez et al., 2009;
420 Gutierrez et al., 2012; Lakehal et al., 2019a) were applied in all the experiments. Seedlings
421 were etiolated in the dark until the hypocotyls were approximatively 6-7 mm long, then were
422 grown in long-day conditions (16 h light 22° C/ 8h dark 17° C cycles, with 130-140 µmol
423 photons/m^2/sec during light phases and constant 65% relative humidity). After 7 days, numbers
424 of primordia and emerged ARs were counted under a binocular stereomicroscope. Numbers of
425 visible LRs were also counted, and the primary root length was measured using ImageJ software
426 (Schindelin et al., 2012). The LR density was calculated by dividing the number of LR by the
427 primary root length.

428

429 **RNA isolation and cDNA synthesis**

430 Total RNA was prepared using a RNAqueous® Total RNA Isolation kit (Ambion™). Portions
431 (4 µg) of the resulting RNA preparations were treated with DNaseI using a DNA*free* Kit
432 (Ambion™) then cDNA was synthesized by reverse transcription using a SuperScript II

433 Reverse transcriptase kit (Invitrogen) with anchored-oligo(dT)$_{18}$ primers, according to the
434 manufacturer's instructions.
435
436 **Quantitative RT-PCR (qRT-PCR) experiments**
437 Transcript levels were assessed by qRT-PCR, in assays with triplicate reaction mixtures (final
438 volume, 20 µL) containing 5 µL of cDNA, 0.5 µM of both forward and reverse primers, and 1×
439 LightCycler 480 SYBR Green I Master (Roche) using a LightCycler 480 instrument (Roche)
440 according to the manufacturer's instructions. A melting curve analytical step was added to each
441 PCR program. The sequences of primers used for all target genes are presented in Supplemental
442 Table 2. The crossing threshold (CT) values for each sample were acquired with the
443 LightCycler 480 software (Roche) using the second derivative maximum method. All
444 quantifications were repeated with at least two independent biological replicates.
445
446 **qRT-PCR data analysis**
447 Reference genes were validated as the most stably expressed genes in our experimental
448 procedures (Gutierrez et al., 2009) using GenNorm software and the most stable two (*TIP41*
449 and *EF1A*) were used to normalize the quantitative qPCR data. The data obtained using both
450 reference genes were similar and only data obtained using *TIP41* are presented here. Relative
451 transcript amounts were calculated as previously described (Gutierrez et al., 2009), and
452 considered significant if fold differences were ≥ 1.5 with p-values ≤ 0.05).
453
454 **RNA sequencing and transcriptomic analysis**
455 Total RNA was extracted from etiolated hypocotyls grown in darkness at T0, just before
456 exposure of some of the etiolated seedlings to light. Further samples were collected after 9 and
457 24 h in long-day conditions (T9L and T24L, respectively). In each case three biological
458 replicates were prepared, and the total RNA was treated with DNaseI using a DNA*free* Kit
459 (Ambion™) to remove any contaminating DNA. The RNA's integrity and quantity were
460 checked using a 2100 Bioanalyzer (Agilent), then it was sequenced by BGI Tech (China) using
461 an Illumina HiSeq 4000 platform. The reads were trimmed with SOAPnuke then clean reads
462 were mapped to the Araport11 reference sequence using Bowtie2 (Langmead and Salzberg,
463 2012). Gene expression was quantified using RSEM (RNA-Seq by Expectation-Maximization)
464 (Li and Dewey, 2014) and differentially expressed genes (DEGs) between *ninja-1myc2-322B*
465 and wild-type plants at selected time points were detected using NOISeq software (Tarazona et
466 al., 2011) with fold change ≥ 2 and probability 0.8 settings.

467 FIMO tools were used, via the http://meme-suite.org/tools/fimo web interface, to scan
468 promoters (1 Kb upstream of ATG translation start codons) of the DEGs for G box and G-box-
469 like motifs with a 1E-4 *p*-value setting.
470
471 **Spatiotemporal gene expression patterns during AR initiation**
472 The spatiotemporal patterns of *NINJA*, *MYC2* and *ERF115* genes' expression during AR
473 initiation were monitored by GUS-based analysis, as follows. Seedlings expressing
474 *pNINJA:GUSplus*, *pMYC2:GUSplus* or *pERF115:GUS* were grown in AR-inducing conditions
475 as described above, then stained with X-GLCA (Duchefa Biochemie, X1405.1000) as
476 previously described (Sorin et al., 2005). At least 25 seedlings of each genotype sampled at
477 each time point were stained, and one representative seedling of each set was photographed.
478
479 **Sample preparation for hormone quantification**
480 Hypocotyls were collected from seedlings grown in AR-inducing conditions as described
481 above. The hypocotyls were quickly dried on tissue paper then frozen in liquid nitrogen.
482 Samples were prepared from six biological replicates.
483
484 **Quantification of *cis*-OPDA, JA and JA-Ile**
485 Endogenous levels of jasmonates (*cis*-OPDA, free JA, and JA-Ile) were determined in 20 mg
486 samples, as previously described (Floková et al., 2014).
487
488 **Quantification of endogenous cytokinin bases**
489 Cytokinin metabolites were quantified following published methodology (Svačinová et al.,
490 2012; Antoniadi et al., 2015) Briefly, samples (20 mg FW) were homogenized and extracted in
491 1 ml of modified Bieleski solvent (60% MeOH, 10% HCOOH and 30% H_2O) together with a
492 cocktail of stable isotope-labelled internal standards (0.25 pmol of CK bases added per sample).
493 The extracts were applied to an Oasis MCX column (30 mg/ml, Waters) conditioned with 1 ml
494 each of 100% MeOH and H_2O, equilibrated sequentially with 1 ml of 50% (v/v) nitric acid, 1
495 ml of H_2O, and 1 ml of 1 M HCOOH, then washed with 1 ml of 1 M HCOOH and 1 ml 100%
496 MeOH. Analytes were then eluted in two steps with 1 ml of 0.35 M aqueous NH_4OH solution
497 and 2 ml of 0.35 M NH_4OH in 60% (v/v) MeOH solution, evaporated to dryness *in vacuo* and
498 stored at -20°C. Cytokinin levels were determined by ultra-high performance liquid
499 chromatography-electrospray tandem mass spectrometry (UHPLC-MS/MS) using stable

500 isotope-labelled internal standards as reference compounds (Rittenberg D., 1940). Following
501 separation with an Acquity UPLC® system (Waters, Milford, MA, USA) equipped with an
502 Acquity UPLC BEH Shield RP18 column (150x2.1 mm dimensions, 1.7 µm particles; Waters),
503 the effluent was introduced into the electrospray ion source of a Xevo™ TQ-S MS triple
504 quadrupole mass spectrometer (Waters). Six independent biological replicates of each genotype
505 sampled at each time point were analyzed.
506
507 **Confocal Laser Scanning Microscopy (cLSM) analysis**
508 Images of the vasculature in *Arabidopsis* hypocotyls at depths up to 150 µm from the epidermal
509 surface were acquired using a Zeiss LSM880 inverted confocal laser scanning microscope (Carl
510 Zeiss GmbH, Oberkochen, Germany) equipped with a C-Achroplan 32x/0.85 W Corr M27 lens.
511 The seedlings were etiolated in the dark until their hypocotyls were 6-7 mm long then incubated
512 in liquid medium containing 30 µg/ml propidium iodide (PI) as a cell wall counter-stain to
513 identify the cell layers, and observed while still alive, mounted with the same medium. The PI
514 was excited using a 561 nm laser while expressed reporter protein (mCITRINE) was excited
515 with a 488 nm Argon laser, using a MBS 488/561 Main Beam Splitter. PI Fluorescence from
516 PI and the reporter (mCITRINE) were detected to localize expression with a photomultiplier
517 tube (PMT) detector and a GaAsP (gallium arsenide phosphide photomultiplier tube) 32-
518 channels spectral detector (with about two times higher sensitivity than the PMT, enabling
519 detection of even poorly expressed reporters), respectively. 3D projections and orthogonal
520 views were generated using FIJI/Image J (Schindelin et al., 2012), including image-wide
521 adjustments of brightness and contrast for each channel before merging to ensure that both
522 signals from PI and the fluorescent protein reporter could be easily seen in all displayed images.
523
524
525
526
527
528
529
530
531
532
533

FUNDING

This work was supported by grants from the Swedish Research Council (VR), the Swedish Research Council for Research and Innovation for Sustainable Growth (VINNOVA), the K & A Wallenberg Foundation, the Carl Trygger Foundation, and the Carl Kempe Foundation awarded to C.B, together with grants from the Ministry of Education, Youth and Sports of the Czech Republic (European Regional Development Fund-Project "Plants as a tool for sustainable global development" No. CZ.02.1.01/0.0/0.0/16_019/0000827), and the Czech Science Foundation (Project No. 19-00973S) awarded to O.N.

ACKNOWLEDGMENTS

The authors sincerely thank Hana Martínková and Petra Amakorová for their help with phytohormone analyses, Nicolas Delhomme and Iryna Shutava from the UPSC bioinformatic platform for their advice and help with the RNA-Seq data analysis and *cis*-regulatory motif search.

AUTHORS' CONTRIBUTIONS

Methodology, A.L., C.B., A.D. Investigation, A.L., A.D., Z.R., S.A., S.E., O.N. Writing – original Draft, A.L., A.D. Writing –Review & Editing, A.L., C.B.; Conceptualization, A.L. C.B.; Supervision, C.B.; Funding Acquisition, C.B., H.T., O.N. and M.S.

555 **REFERENCES**

556 **Acosta, I. F., Gasperini, D., Chételat, A., Stolz, S., Santuari, L., and Farmer, E. E.**
557 (2013). Role of NINJA in root jasmonate signaling. Proc. Natl. Acad. Sci. U S A
558 **110**:15473–15478.

559 **An, C., Li, L., Zhai, Q., You, Y., Deng, L., Wu, F., Chen, R., Jiang, H., Wang, H., Chen,**
560 **Q., et al.** (2017). Mediator subunit MED25 links the jasmonate receptor to
561 transcriptionally active chromatin. Proc. Natl. Acad. Sci. U S A **114**:E8930–E8939.

562 **Andersen, T. G., Naseer, S., Ursache, R., Wybouw, B., Smet, W., De Rybel, B., Vermeer,**
563 **J. E. M., and Geldner, N.** (2018). Diffusible repression of cytokinin signalling produces
564 endodermal symmetry and passage cells. Nature **555**:529–533.

565 **Antoniadi, I., Plačková, L., Simonovik, B., Doležal, K., Turnbull, C., Ljung, K., and**
566 **Novák, O.** (2015). Cell-type-specific cytokinin distribution within the arabidopsis
567 primary root apex. Plant Cell **27**:1955–1967.

568 **Asahina, M., Azuma, K., Pitaksaringkarn, W., Yamazaki, T., Mitsuda, N., Ohme-**
569 **Takagi, M., Yamaguchi, S., Kamiya, Y., Okada, K., Nishimura, T., et al.** (2011).
570 Spatially selective hormonal control of RAP2.6L and ANAC071 transcription factors
571 involved in tissue reunion in Arabidopsis. Proc. Natl. Acad. Sci. U S A **108**:16128–
572 16132.

573 **Bellini, C., Pacurar, D. I., and Perrone, I.** (2014). Adventitious Roots and Lateral Roots:
574 Similarities and Differences. Annu. Rev. Plant Biol. **65**:639–666.

575 **Campos, M. L., Yoshida, Y., Major, I. T., De Oliveira Ferreira, D., Weraduwage, S. M.,**
576 **Froehlich, J. E., Johnson, B. F., Kramer, D. M., Jander, G., Sharkey, T. D., et al.**
577 (2016). Rewiring of jasmonate and phytochrome B signalling uncouples plant growth-
578 defense tradeoffs. Nat. Commun. **7**:1–10.

579 **Causier, B., Ashworth, M., Guo, W., and Davies, B.** (2012). The TOPLESS interactome: A
580 framework for gene repression in Arabidopsis. Plant Phys. **158**:423–438.

581 **Che, P., Lall, S., Nettleton, D., and Howell, S. H.** (2006). Gene expression programs during
582 shoot, root, and callus development in Arabidopsis tissue culture. Plant Phys. **141**:620–
583 637.

584 **Chen, R., Jiang, H., Li, L., Zhai, Q., Qi, L., Zhou, W., Liu, X., Li, H., Zheng, W., Sun, J.,**
585 **et al.** (2012). The arabidopsis Mediator subunit MED25 differentially regulates
586 jasmonate and abscisic acid signaling through interacting with the MYC2 and ABI5
587 transcription factors. Plant Cell **24**:2898–2916.

588 **Chini, A., Fonseca, S., Fernández, G., Adie, B., Chico, J. M., Lorenzo, O., García-**

589 **Casado, G., López-Vidriero, I., Lozano, F. M., Ponce, M. R., et al.** (2007). The JAZ
590 family of repressors is the missing link in jasmonate signalling. Nature **448**:666–671.
591 **Chini, A., Gimenez-Ibanez, S., Goossens, A., and Solano, R.** (2016). Redundancy and
592 specificity in jasmonate signalling. Curr. Opin. Plant Biol. **33**:147–156.
593 **Clough, S. J., and Bent, A. F.** (1998). Floral dip: A simplified method for Agrobacterium-
594 mediated transformation of Arabidopsis thaliana. Plant J. **16**:735–743.
595 **De Rybel, B., Vassileva, V., Parizot, B., Demeulenaere, M., Grunewald, W., Audenaert,**
596 **D., Van Campenhout, J., Overvoorde, P., Jansen, L., Vanneste, S., et al.** (2010). A
597 novel Aux/IAA28 signaling cascade activates GATA23-dependent specification of
598 lateral root founder cell identity. Curr. Biol. **20**:1697–1706.
599 **Floková, K., Tarkowská, D., Miersch, O., Strnad, M., Wasternack, C., and Novák, O.**
600 (2014). UHPLC-MS/MS based target profiling of stress-induced phytohormones.
601 Phytochemistry **105**:147–157.
602 **Fonseca, S., Chini, A., Hamberg, M., Adie, B., Porzel, A., Kramell, R., Miersch, O.,**
603 **Wasternack, C., and Solano, R.** (2009). (+)-7-iso-Jasmonoyl-L-isoleucine is the
604 endogenous bioactive jasmonate. Nat. Chem. Biol. **5**:344–350.
605 **Gasperini, D., Chételat, A., Acosta, I. F., Goossens, J., Pauwels, L., Goossens, A., Dreos,**
606 **R., Alfonso, E., and Farmer, E. E.** (2015). Multilayered Organization of Jasmonate
607 Signalling in the Regulation of Root Growth. PLoS Genet. **11**:1–27.
608 **Godoy, M., Franco-Zorrilla, J. M., Pérez-Pérez, J., Oliveros, J. C., Lorenzo, Ó., and**
609 **Solano, R.** (2011). Improved protein-binding microarrays for the identification of DNA-
610 binding specificities of transcription factors. Plant J. **66**:700–711.
611 **Guo, Q., Yoshida, Y., Major, I. T., Wang, K., Sugimoto, K., Kapali, G., Havko, N. E.,**
612 **Benning, C., and Howe, G. A.** (2018). JAZ repressors of metabolic defense promote
613 growth and reproductive fitness in Arabidopsis. Proc. Natl. Acad. Sci. U S A
614 **115**:E10768–E10777.
615 **Gutierrez, L., Bussell, J. D., Pacurar, D. I., Schwambach, J., Pacurar, M., and Bellini, C.**
616 (2009). Phenotypic Plasticity of Adventitious Rooting in Arabidopsis Is Controlled by
617 Complex Regulation of AUXIN RESPONSE FACTOR Transcripts and MicroRNA
618 Abundance. Plant Cell **21**:3119–3132.
619 **Gutierrez, L., Mongelard, G., Floková, K., Păcurar, D. I., Novák, O., Staswick, P.,**
620 **Kowalczyk, M., Păcurar, M., Demailly, H., Geiss, G., et al.** (2012). Auxin Controls
621 Arabidopsis Adventitious Root Initiation by Regulating Jasmonic Acid Homeostasis.
622 Plant Cell **24**:2515–2527.

623 **Heyman, J., Cools, T., Vandenbussche, F., Heyndrickx, K. S., Van Leene, J.,**
624 **Vercauteren, I., Vanderauwera, S., Vandepoele, K., De Jaeger, G., Van Der**
625 **Straeten, D., et al.** (2013). ERF115 controls root quiescent center cell division and stem
626 cell replenishment. Science **342**:860–863.
627 **Heyman, J., Cools, T., Canher, B., Shavialenka, S., Traas, J., Vercauteren, I., Van Den**
628 **Daele, H., Persiau, G., De Jaeger, G., Sugimoto, K., et al.** (2016). The heterodimeric
629 transcription factor complex ERF115-PAT1 grants regeneration competence. Nat. Plants
630 **2**:1–7.
631 **Heyman, J., Canher, B., Bisht, A., Christiaens, F., and De Veylder, L.** (2018). Emerging
632 role of the plant ERF transcription factors in coordinating wound defense responses and
633 repair. J. Cell Sci. **131**:1-8
634 **Ikeuchi, M., Iwase, A., Rymen, B., Lambolez, A., Kojima, M., Takebayashi, Y., Heyman,**
635 **J., Watanabe, S., Seo, M., De Veylder, L., et al.** (2017). Wounding triggers callus
636 formation via dynamic hormonal and transcriptional changes. Plant Phys. **175**:1158–
637 1174.
638 **Ikeuchi, M., Shibata, M., Rymen, B., Iwase, A., Bgman, A. M., Watt, L., Coleman, D.,**
639 **Favero, D. S., Takahashi, T., Ahnert, S. E., et al.** (2018). A Gene Regulatory Network
640 for Cellular Reprogramming in Plant Regeneration. Plant Cell Physiol. **59**:765–777.
641 **Ikeuchi, M., Favero, D. S., Sakamoto, Y., Iwase, A., Coleman, D., Rymen, B., and**
642 **Sugimoto, K.** (2019). Molecular Mechanisms of Plant Regeneration. Annu. Rev. Plant
643 Biol. **70**:377–406.
644 **Kagale, S., Links, M. G., and Rozwadowski, K.** (2010). Genome-wide analysis of ethylene-
645 responsive element binding factor-associated amphiphilic repression motif-containing
646 transcriptional regulators in arabidopsis. Plant Phys. **152**:1109–1134.
647 **Kong, X., Tian, H., Yu, Q., Zhang, F., Wang, R., Gao, S., Xu, W., Liu, J., Shani, E., Fu,**
648 **C., et al.** (2018). PHB3 Maintains Root Stem Cell Niche Identity through ROS-
649 Responsive AP2/ERF Transcription Factors in Arabidopsis. Cell Rep. **22**:1350–1363.
650 **Kumar S., Stecher G., Li M., Knyaz C., and Tamura K.** (2018). MEGA X: Molecular
651 Evolutionary Genetics Analysis across computing platforms. *Mol. Biol. Evol.* **35**:1547-
652 1549.
653 **Kuroha, T., Tokunaga, H., Kojima, M., Ueda, N., Ishida, T., Nagawa, S., Fukuda, H.,**
654 **Sugimoto, K., and Sakakibara, H.** (2009). Functional analyses of LONELY GUY
655 cytokinin-activating enzymes reveal the importance of the direct activation pathway in
656 Arabidopsis. Plant Cell **21**:3152–3169.

657 **Lakehal, A., and Bellini, C.** (2018). Control of adventitious root formation: insights into
658 synergistic and antagonistic hormonal interactions. Physiol Plant. **165**:90–100.
659 **Lakehal, A., Chaabouni, S., Cavel, E., Le Hir, R., Ranjan, A., Raneshan, Z., Novák, O.,**
660 **Păcurar, D. I., Perrone, I., Jobert, F., et al.** (2019a). A Molecular Framework for the
661 Control of Adventitious Rooting by TIR1/AFB2-Aux/IAA-Dependent Auxin Signaling
662 in Arabidopsis. Mol. Plant **12**:1499–1514.
663 **Lakehal, A., Dob, A., Novák, O., and Bellini, C.** (2019b). A DAO1-Mediated Circuit
664 Controls Auxin and Jasmonate Crosstalk Robustness during Adventitious Root Initiation
665 in Arabidopsis. Int. J. Mol. Sci. **20**:4428.
666 **Lakehal, A., Ranjan, A., and Bellini, C.** (2020). Multiple Roles of Jasmonates in Shaping
667 Rhizotaxis: Emerging Integrators. In: Champion A., Laplaze L. (eds) Jasmonate in Plant
668 Biology. Methods Mol. Biol., Humana, New York, NY **2085**:3–22.
669 **Langmead, B., and Salzberg, S. L.** (2012). Fast gapped-read alignment with Bowtie 2. Nat.
670 Methods **9**:357–359.
671 **Li, B., and Dewey, C. N.** (2014). RSEM: Accurate transcript quantification from RNA-seq
672 data with or without a reference genome. BMC Bioinformatics **12**:41–74.
673 **Mehrnia, M., Balazadeh, S., Zanor, M. I., and Mueller-Roeber, B.** (2013). EBE, an
674 AP2/ERF transcription factor highly expressed in proliferating cells, affects shoot
675 architecture in Arabidopsis. Plant Phys. **162**:842–857.
676 **Miyawaki, K., Tarkowski, P., Matsumoto-Kitano, M., Kato, T., Sato, S., Tarkowska, D.,**
677 **Tabata, S., Sandberg, G., and Kakimoto, T.** (2006). Roles of Arabidopsis ATP/ADP
678 isopentenyltransferases and tRNA isopentenyltransferases in cytokinin biosynthesis.
679 Proc. Natl. Acad. Sci. U S A **103**:16598–16603.
680 **Nakano, T., Suzuki, K., Fujimura, T., and Shinshi, H.** (2006). Genome-wide analysis of
681 the ERF gene family in arabidopsis and rice. Plant Phys. **140**:411–432.
682 **Pauwels, L., Barbero, G. F., Geerinck, J., Tilleman, S., Grunewald, W., Pérez, A. C.,**
683 **Chico, J. M., Bossche, R. Vanden, Sewell, J., Gil, E., et al.** (2010). NINJA connects
684 the co-repressor TOPLESS to jasmonate signalling. Nature **464**:788–791.
685 **Rittenberg D., Foster. G. L.** (1940). A new procedure for quantitative analysis by Isotope
686 dilution, with application to the determination of amino acids and fatty acids. J. Biol.
687 Chem. **133**:737–744.
688 **Schindelin, J., Arganda-Carreras, I., Frise, E., Kaynig, V., Longair, M., Pietzsch, T.,**
689 **Preibisch, S., Rueden, C., Saalfeld, S., Schmid, B., et al.** (2012). Fiji: an open-source
690 platform for biological-image analysis. Nat. methods **9**:676–82.

691 **Sheard, L. B., Tan, X., Mao, H., Withers, J., Ben-Nissan, G., Hinds, T. R., Kobayashi,**
692 **Y., Hsu, F. F., Sharon, M., Browse, J., et al.** (2010). Jasmonate perception by inositol-
693 phosphate-potentiated COI1-JAZ co-receptor. Nature **468**:400–407.
694 **Shyu, C., Figueroa, P., DePew, C. L., Cooke, T. F., Sheard, L. B., Moreno, J. E., Katsir,**
695 **L., Zheng, N., Browse, J., and Howe, G. A.** (2012). JAZ8 Lacks a Canonical Degron
696 and Has an EAR Motif That Mediates Transcriptional Repression of Jasmonate
697 Responses in Arabidopsis. Plant Cell **24**:536–550.
698 **Smolen, G. A., Pawlowski, L., Wilensky, S. E., and Bender, J.** (2002). Dominant alleles of
699 the basic helix-loop-helix transcription factor ATR2 activate stress-responsive genes in
700 arabidopsis. Genetics **161**:1235–1246.
701 **Sorin, C., Bussell, J. D., Camus, I., Ljung, K., Kowalczyk, M., Geiss, G., McKhann, H.,**
702 **Garcion, C., Vaucheret, H., Sandberg, G., et al.** (2005). Auxin and Light Control of
703 Adventitious Rooting in Arabidopsis. Plant Cell **17**:1343–1359.
704 **Staswick, P. E., Sut, W., and Howell, S. H.** (1992). Methyl jasmonate inhibition of root
705 growth and induction of a leaf protein are decreased in an Arabidopsis thaliana mutant.
706 Proc. Natl. Acad. Sci. USA **89**:6837–6840.
707 **Steffens, B., and Rasmussen, A.** (2016). The Physiology of Adventitious Roots. Plant Phys.
708 **170**:603–617.
709 **Sukumar, P., Maloney, G. S., and Muday, G. K.** (2013). Localized Induction of the ATP-
710 Binding Cassette B19 Auxin Transporter Enhances Adventitious Root Formation in
711 Arabidopsis. Plant Phys. **162**:1392–1405.
712 **Svačinová, J., Novák, O., Plačková, L., Lenobel, R., Holík, J., Strnad, M., and Doležal,**
713 **K.** (2012). A new approach for cytokinin isolation from Arabidopsis tissues using
714 miniaturized purification: pipette tip solid-phase extraction. Plant Methods **8**:1–14.
715 **Tarazona S., Garcıa-Alcalde F., Dopazo J., Ferrer A., and Conesa A.** (2011). Differential
716 expression in RNA-seq: A matter of depth. Genome Res. **21**:2213–2223.
717 **Thines, B., Katsir, L., Melotto, M., Niu, Y., Mandaokar, A., Liu, G., Nomura, K., He, S.**
718 **Y., Howe, G. A., and Browse, J.** (2007). JAZ repressor proteins are targets of the
719 SCFCOI1 complex during jasmonate signalling. Nature **448**:661–665.
720 **Thireault, C., Shyu, C., Yoshida, Y., St. Aubin, B., Campos, M. L., and Howe, G. A.**
721 (2015). Repression of jasmonate signaling by a non-TIFY JAZ protein in Arabidopsis.
722 Plant J. **82**:669–679.
723 **Wang, Z. P., Xing, H. L., Dong, L., Zhang, H. Y., Han, C. Y., Wang, X. C., and Chen, Q.**
724 **J.** (2015). Egg cell-specific promoter-controlled CRISPR/Cas9 efficiently generates

725 homozygous mutants for multiple target genes in Arabidopsis in a single generation.
726 Genome Biol. **16**:1–12.
727 **Wasternack, C., and Hause, B.** (2013). Jasmonates: Biosynthesis, perception, signal
728 transduction and action in plant stress response, growth and development. An update to
729 the 2007 review in Annals of Botany. Ann. Bot. **111**:1021–1058.
730 **Werner, T., Motyka, V., Laucou, V., Smets, R., Van Onckelen, H., and Schmülling, T.**
731 (2003). Cytokinin-Deficient Transgenic Arabidopsis Plants Show Multiple
732 Developmental Alterations Indicating Opposite Functions of Cytokinins in the
733 Regulation of Shoot and Root Meristem Activity. Plant Cell **15**:2532–2550.
734 **Xie, D. X., Feys, B. F., James, S., Nieto-Rostro, M., and Turner, J. G.** (1998). COI1: An
735 Arabidopsis gene required for jasmonate-regulated defense and fertility. Science
736 **280**:1091–1094.
737 **Xing, H.-L., Wang, Z.-P., Zhang, H.-Y., Han, C.-Y., Liu, B., Wang, X.-C., Chen, Q.-J.,**
738 **and Dong, L.** (2014). A CRISPR/Cas9 toolkit for multiplex genome editing in plants.
739 BMC Plant Biol. **14**:372.
740 **Yan, Y., Stolz, S., Chételat, A., Reymond, P., Pagni, M., Dubugnon, L., and Farmer, E.**
741 **E.** (2007). A downstream mediator in the growth repression limb of the jasmonate
742 pathway. Plant Cell **19**:2470–2483.
743 **Yang, S., Poretska, O., and Sieberer, T.** (2018). ALTERED MERISTEM PROGRAM1
744 restricts shoot meristem proliferation and regeneration by limiting HD-ZIP III-mediated
745 expression of RAP2.6l. Plant Phys. **177**:1580–1594.
746 **Zhang, F., Yao, J., Ke, J., Zhang, L., Lam, V. Q., Xin, X. F., Zhou, X. E., Chen, J.,**
747 **Brunzelle, J., Griffin, P. R., et al.** (2015). Structural basis of JAZ repression of MYC
748 transcription factors in jasmonate signalling. Nature **525**:269–273.
749 **Zhang, G., Zhao, F., Chen, L., Pan, Y., Sun, L., Bao, N., Zhang, T., Cui, C. X., Qiu, Z.,**
750 **Zhang, Y., et al.** (2019). Jasmonate-mediated wound signalling promotes plant
751 regeneration. Nat. Plants **5**:491–497.
752 **Zhou, W., Lozano-Torres, J. L., Blilou, I., Zhang, X., Zhai, Q., Smant, G., Li, C., and**
753 **Scheres, B.** (2019). A Jasmonate Signaling Network Activates Root Stem Cells and
754 Promotes Regeneration. Cell **177**:942-956.e14.
755 **Zhu, Z., An, F., Feng, Y., Li, P., Xue, L., A, M., Jiang, Z., Kim, J.-M., To, T. K., Li, W.,**
756 **et al.** (2011). Derepression of ethylene-stabilized transcription factors (EIN3/EIL1)
757 mediates jasmonate and ethylene signaling synergy in Arabidopsis. Proc. Natl. Acad.
758 Sci. U S A **108**:12539–12544.
759

760 **FIGURE LEGENDS**

761

762 **Figure 1: A genetic model for the action of JA signaling components during ARI**. With a
763 low auxin signaling input, the JA pool increases in the hypocotyl. This triggers degradation of
764 the targeted JAZs, thereby releasing transcriptional activity of the MYC2, 3, 4 and inhibiting
765 ARI. With a high auxin signaling input, the JA pool decreases in the hypocotyl, thereby
766 repressing the MYC-mediated JA signaling machinery and increasing ARI (Gutierrez et al.,
767 2012; Lakehal et al., 2019a).

768

769 **Figure 2: JA signaling inhibits ARI in NINJA-dependent and -independent manners.**
770 (A) Average number of ARs observed in indicated multiple *jaz* mutants and wild-type (Col-0)
771 seedlings. Data are pooled and averaged numbers observed in three biological replicates of at
772 least 40 seedlings. One-way ANOVA combined with Tukey's multiple comparison post-tests
773 showed that the *jaz1jaz3jaz4jaz9jaz10* produced significantly more ARs than wild-type plants.
774 Error bars indicate ± SEM ($n \geq 40$; $P < 0.05$).
775 (B) Average number of ARs produced by JA signaling mutants. A non-parametric Kruskal-
776 Wallis test followed by Dunn's multiple comparison test indicated that mutations in the *MYC2*
777 or *NINJA* genes result in significant differences in AR number, relative to wild-type numbers.
778 Error bars indicate ± SEM ($n \geq 40$; $P < 0.02$). Values marked with asterisks significantly differ
779 from corresponding wild-type values and those marked with hash signs significantly differ from
780 values obtained for the single *ninja-1 or ninja-2* mutants.
781 (C) Lateral root density of JA signaling mutants and wild-type seedlings grown in AR
782 phenotyping conditions. One-way ANOVA combined with Tukey's multiple comparison post-
783 test indicated that the *myc2-322B* and *ninja-1myc2-322B* mutants had slightly lower and
784 slightly higher than wild-type LR densities, respectively. Error bars indicate ± SEM ($n \geq 40$; P
785 < 0.05).
786 (D) to (E) Representative photos of (D) wild-type and (E) *ninja-1myc2-322B* double mutant
787 seedlings. Scale bars represent 6 mm. Arrowheads indicate hypocotyl-root junctions (white) or
788 ARs (red).

789

790

791

792

793

794 **Figure 3: NINJA-dependent JA signaling inhibit ARI in pericycle cells.**
795 (A) to (E) Spatiotemporal activity patterns of the *NINJA* and *MYC2* promoters, left and right,
796 respectively in each panel. Seedlings expressing the *pNINJA:GUSplus* or *pMYC2:GUSplus*
797 constructs were grown in the dark until their hypocotyls were 6-7 mm long (T0) (A) then either
798 kept in the dark for 9 h (T9D) (B) and 24 h (T24D) (C) or transferred to the light for 9 h (T9L)
799 (D) or 24 h (T24L) (E). Scale bars represent 6 mm.
800 (F) to (H) Representative images of etiolated hypocotyls expressing
801 *pNINJA:NINJA:mCITRINE* (F), *pGATA23:NINJA:mCITRINE* (G), and
802 *pXPP:NINJA:mCITRINE* (H) of seedlings grown in darkness until their hypocotyls were 6-7
803 mm long. The cell walls were counterstained magenta with propidium iodide (PI). Orthogonal
804 views from epidermis to vasculature are shown in the top panels. Z-projections of the hypocotyl
805 volume around the vasculature are shown in the bottom panels. The following cell types can be
806 distinguished: Epidermis (Ep), Cortex (Co), Endodermis (En), Pericycle (Pe) and Xylem (Xy).
807 In orthogonal views, the two protoxylem elements allow deduction of the direction of the xylem
808 axis and thus the position of the xylem-pole pericycle. Arrowheads indicate signals in xylem-
809 pole pericycle cells in green.
810 (I) Average numbers of ARs produced by the *ninja-1myc2-322B* double mutant, two
811 independent transgenic lines expressing *pXPP:NINJA:mCITRINE/ninja-1myc2-322B* or
812 *pGATA23:NINJA:mCITRINE/ninja-1myc2-322B* and wild-type (Col-0) seedlings. A non-
813 parametric Kruskal-Wallis test followed by Dunn's multiple comparison post-test indicated that
814 *pXPP:NINJA:mCITRINE/ninja-1myc2-322B* (#14.7 and #11.3) and
815 *pGATA23:NINJA:mCITRINE/ninja-1myc2-322B* (#2.4 and #5.8) produced significantly more
816 ARs than the *ninja1myc2-322B* double mutant. Error bars indicate ± SEM ($n \geq 30$; $P < 0.006$).
817
818 **Figure 4: RNA-Seq revealed several DEGs between the *ninja-1myc2-322B* double mutant**
819 **and wild-type seedlings**.
820 **(**A) Schematic representation of the RNA-Seq experiment. Total RNA was extracted from
821 hypocotyls of *ninja-1myc2-322B* double mutant and wild-type seedlings grown in the dark until
822 their hypocotyls were 6-7 mm long (T0), and after their transfer to the light for 9 h (T9) or 24
823 h (T24).
824 (B) Venn diagram summarizing the DEGs between *ninja-1myc2-322B* double mutant and wild-
825 type seedlings. (C) Enrichment of G-box (CACGTG, CACATG) or G-box-like (AACGTG,
826 CATGTG CACGCG or CACGAG) motifs in the DEGs. Colors indicate upregulated genes

827 (red) or downregulated genes (blue) containing at least one of the motifs. The gray color
828 indicates the remaining DEGs, containing none of the mentioned motifs.
829 (D) Heatmap of expression of the 13 *JAZ* genes. The map is based on fold-differences (log_2) in
830 transcript abundance (based on RNA-Seq data) in *ninja-1myc2-322B* double mutant samples
831 relative to the abundance in wild-type samples. Colors indicate upregulated genes (red) and
832 downregulated genes (blue) in *ninja-1myc2-322B* double mutant relative to expression levels
833 in wild-type seedlings. Values marked with asterisks are statistically significant.
834 (E) Heatmap of expression selected JA biosynthesis genes. The map is based on fold-
835 differences (log_2) in transcript abundance (based on RNA-Seq data) in *ninja-1myc2-322B*
836 double mutant samples relative to the abundance in wild-type samples. Colors indicate
837 upregulated genes (red) and downregulated genes (blue) in *ninja-1myc2-322B* relative to wild-
838 type expression levels. Values marked with asterisks are statistically significant.
839 (F) to (H) Endogenous jasmonate contents. (F) *cis*-OPDA, (G) free JA and (H) JA-Ile contents
840 of hypocotyls of *ninja-1myc2-322B* and wild-type seedlings grown in the dark until their
841 hypocotyls were 6 mm long (T0) and after their transfer to the light for 9 h (T9) and 24 h (T24).
842 Asterisks indicate statistically significant differences between the mutant lines and wild-type
843 plants according to ANOVA analysis (*, **, and *** indicate p values of $0.05 > p > 0.01$, 0.01
844 $> p > 0.001$, and $p < 0.001$, respectively). Error bars indicate ± SD of six biological replicates.
845
846 **Figure 5: *ERF113*, *ERF114* and *ERF115* are induced by JA signaling**.
847 **(**A) Heatmap of expression of the subgroup X *ERF family* members. The map is based on fold-
848 differences (log_2) in transcript abundance (based on RNA-Seq data) in *ninja-1myc2-322B*
849 double mutant samples relative to the abundance in wild-type samples. Colors indicate
850 upregulated genes (red) or downregulated genes (blue) in *ninja-1myc2-322B* relative to wild
851 type expression levels. Values marked with asterisks are statistically significant.
852 (B) Phylogenetic tree of subgroup X of the AP2/ERF protein family derived from protein
853 sequence alignment by the maximum likelihood method using MEGA X software (Kumar et
854 al., 2018).
855 (C) Validation by qRT-PCR of mutation-induced shifts in *ERF113*, *ERF114* and *ERF115*
856 expression profiles in the *ninja-1myc2-322B* double mutant (abundance of transcripts, in log10
857 scale, at indicated time points relative to their abundance in wild-type seedlings, which was
858 arbitrarily set to 1). Error bars indicate ±SE obtained from three independent technical
859 replicates. Asterisks mark significance differences between the genotypes according to a *t*-test

860 (P < 0.001, n = 3). The experiment was repeated twice with independent biological replicates
861 and gave similar results.
862
863 **Figure 6: The *ERF115* gene is an inhibitor of ARI.**
864 (A) Average numbers of AR produced by *erf* mutants and wild-type seedlings. One-way
865 ANOVA combined with Tukey's multiple comparison post-test indicated that only the triple
866 mutant *rap2-6lerf114Cerf115* significantly differed in this respect from wild-type (Col-0)
867 plants. Error bars indicate ± SEM (n ≥ 40, P < 0.001).
868 (B) Average numbers of ARs produced by *35S:ERF115* and *pERF115:ERF115:SRDX* relative
869 to numbers produced by wild-type plants. Data from two independent biological replicates,
870 each of at least 40 seedlings, were pooled and averaged. A non-parametric Kruskal-Wallis test
871 followed by Dunn's multiple comparison test indicated that numbers of ARs produced by the
872 transgenic and wild-type plants significantly differed. Error bars indicate ± SEM (n ≥ 40, P <
873 0.02).
874 (C) LR density of *35S:ERF115* and *pERF115:ERF115:SRDX* lines and wild type plants in AR
875 phenotyping conditions. *35S:ERF115* mutants had significantly lower LR density than wild-
876 type plants according to one-way ANOVA followed by Tukey's multiple comparison test.
877 (D) Spatiotemporal activity pattern of the *ERF115* promoter, as shown by seedlings expressing
878 the *pERF115:GUS* construct grown in the dark until their hypocotyls were 6-7 mm long (T0),
879 and 24 h (T24L) after either transfer to the light or further growth in the dark (T24D). Scale
880 bars represent 6 mm.
881 (E) Validation by qRT-PCR of *ERF115* expression patterns in wild-type plants. Presented gene
882 expression values are relative (in log10 scale) to the expression at T0, for which the value was
883 arbitrarily set to 1. Error bars indicate ±SE obtained from three independent technical replicates.
884 A *t*-test indicated that values indicated by an Asterisks indicate values that significantly differ
885 from the T0 values (P < 0.001, n = 3). The experiment was repeated twice with independent
886 biological replicates and gave similar results.
887 (F) to (H) Representative photos of (F) wild-type, (G) *35S:ERF115*, and (H)
888 *pERF115:ERF115:SRDX* seedlings.
889 (I) to (J) Representative photos of wild-type and *35S:ERF115* seedlings grown in the dark until
890 their hypocotyls were 6-7 mm long, then transferred to fresh medium containing either mock
891 solution or 1 µM naphthaleneacetic acid (NAA) for seven more days under long-day conditions
892 to induce ARs. Arrowheads indicate hypocotyl-root junctions (white) or ARs (red). Scale bars
893 represent 6 mm.

894 (K) Average numbers of ARs produced by wild-type and *35S:ERF115* plants in response to
895 NAA. Wild-type seedlings produced significantly more ARs after NAA treatment than after
896 mock-treatment according to a Mann-Whitney test ($n \geq 40$, $P < 0.0001$), but NAA treatment
897 had no significant effect on AR production by *35S:ERF115* plants. Error bars indicate ± SEM.
898
899 **Figure 7: Cytokinins inhibit ARI downstream of *ERF115*.**
900 (A) Average numbers of ARs produced by wild-type (Col-0) seedlings, which were grown in
901 the dark until their hypocotyls were 6-7 mm long, then transferred to fresh medium containing
902 either mock solution or solutions with indicated concentrations of 6-Benzylaminopurine (6-
903 BA). The seedlings were kept for seven more days under long-day conditions to induce ARs.
904 Seedlings treated with 0.25 µM or 0.5 µM 6-BA significantly differed from the mock-treated
905 controls, according to a non-parametric Kruskal-Wallis test followed by Dunn's multiple
906 comparison test. Error bars indicate ± SEM ($n \geq 40$, $P < 0.004$).
907 (B) to (D) Average numbers of ARs produced by wild-type plants and: (B) *ipt3ipt5ipt7* triple
908 mutants defective in CK biosynthesis, (C) *35S:CKX1 CYTOKININ OXIDASE1*-overexpressing
909 plants, which have reduced CK contents due to increased rates of degradation, and (D) CK
910 signaling mutants.
911 (E) Relative amounts of *ARR5* and *ARR7* transcripts quantified by qRT-PCR. Total RNA was
912 extracted from hypocotyls of *35S:ERF115* and the wild-type seedlings grown in AR-inducing
913 conditions, as outlined above, at T0 (at the end of the dark incubation) and T24 (24 hours later).
914 The gene expression values are relative to wild-type values, which were arbitrarily set to 1. The
915 Y axis scale is a $\log_{10}$ scale. Error bars indicate ± SEM obtained from three technical replicates.
916 Asterisks indicate values that significantly differ from wild-type values according to a *t*-test (P
917 < 0.001, $n = 3$). The experiment was repeated once with an independent biological replicate and
918 gave similar results.
919 (F) Endogenous contents of active CK bases. The CK bases were quantified in the hypocotyls
920 of *35S:ERF115* and the wild-type seedlings grown in the dark until they were 6-7 mm long
921 (T0) and after their transfer to the light for 9 h (T9) or 24 h (T24). Asterisks indicate statistically
922 significant differences between mutant and wild-type plants according to ANOVA (*, **, and
923 *** indicate P-values of $0.05 > P > 0.01$, $0.01 > P > 0.001$, and $P < 0.001$, respectively). Error
924 bars indicate ± SD of six biological replicates.
925 (G) Average numbers of ARs produced by *35S:ERF115* plants, *35S:ERF115* plants
926 overexpressing *CKX1* from a *35S:CKX1* construct and the *ipt3,5,7* triple mutant overexpressing
927 *ERF115* from a *35S:ERF115* construct. Numbers produced by the multiple mutants

928 significantly differed from numbers produced by *35S:ERF115* plants according to a non-
929 parametric Kruskal-Wallis test followed by Dunn's multiple comparison test. Error bars
930 indicate ± SEM ($n \geq 40$, $P < 0.0001$).
931
932
933

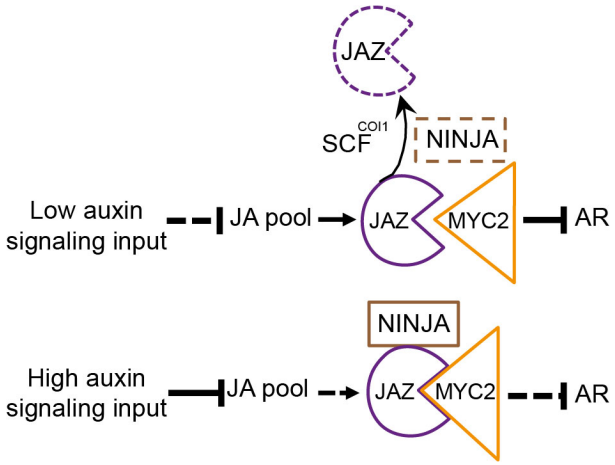

Figure 1: A genetic model for the action of JA signaling components during ARI. With a low auxin signaling input, the JA pool increases in the hypocotyl. This triggers degradation of the targeted JAZs, thereby releasing transcriptional activity of the MYC2, 3, 4 and inhibiting ARI. With a high auxin signaling input, the JA pool decreases in the hypocotyl, thereby repressing the MYC-mediated JA signaling machinery and increasing ARI (Gutierrez et al., 2012; Lakehal et al., 2019a).

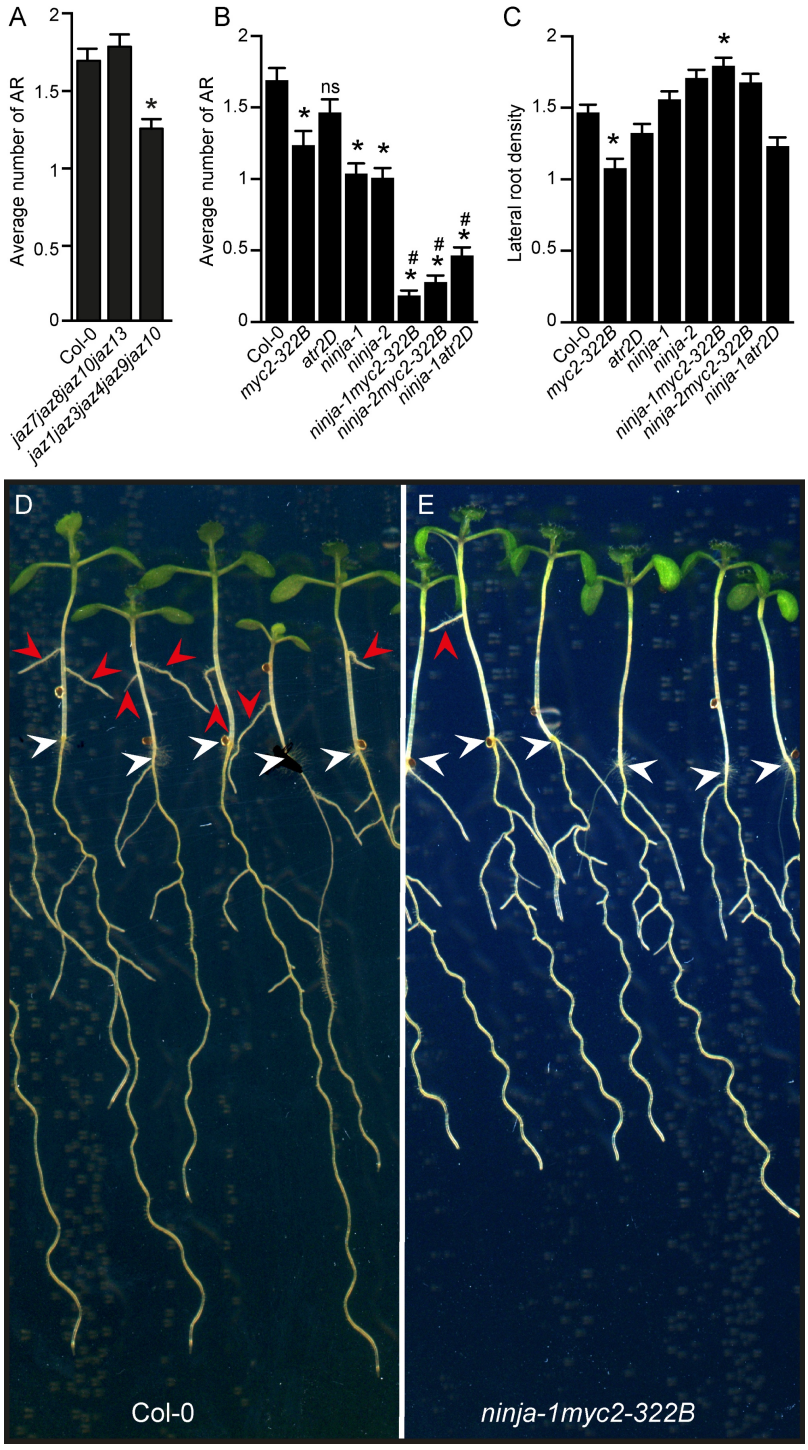

Figure 2: JA signaling inhibits ARI in NINJA-dependent and -independent manners. (A) Average number of ARs observed in indicated multiple *jaz* mutants and wild-type (Col-0) seedlings. Data are pooled and averaged numbers observed in three biological replicates of at least 40 seedlings. One-way ANOVA combined with Tukey's multiple comparison post-tests showed that the *jaz1jaz3jaz4jaz9jaz10* produced significantly more ARs than wild-type plants. Error bars indicate ± SEM ($n \geq 40$; $P < 0.05$). (B) Average number of ARs produced by JA signaling mutants. A non-parametric Kruskal-Wallis test followed by Dunn's multiple

comparison test indicated that mutations in the *MYC2* or *NINJA* genes result in significant differences in AR number, relative to wild-type numbers. Error bars indicate ± SEM ($n \geq 40$; $P < 0.02$). Values marked with asterisks significantly differ from corresponding wild-type values and those marked with hash signs significantly differ from values obtained for the single *ninja-1 or ninja-2* mutants. (C) Lateral root density of JA signaling mutants and wild-type seedlings grown in AR phenotyping conditions. One-way ANOVA combined with Tukey's multiple comparison post-test indicated that the *myc2-322B* and *ninja-1myc2-322B* mutants had slightly lower and slightly higher than wild-type LR densities, respectively. Error bars indicate ± SEM ($n \geq 40$; $P < 0.05$). (D-E) Representative photos of (D) wild-type and (E) *ninja-1myc2-322B* double mutant seedlings. Scale bars represent 6 mm. Arrowheads indicate hypocotyl-root junctions (white) or ARs (red).

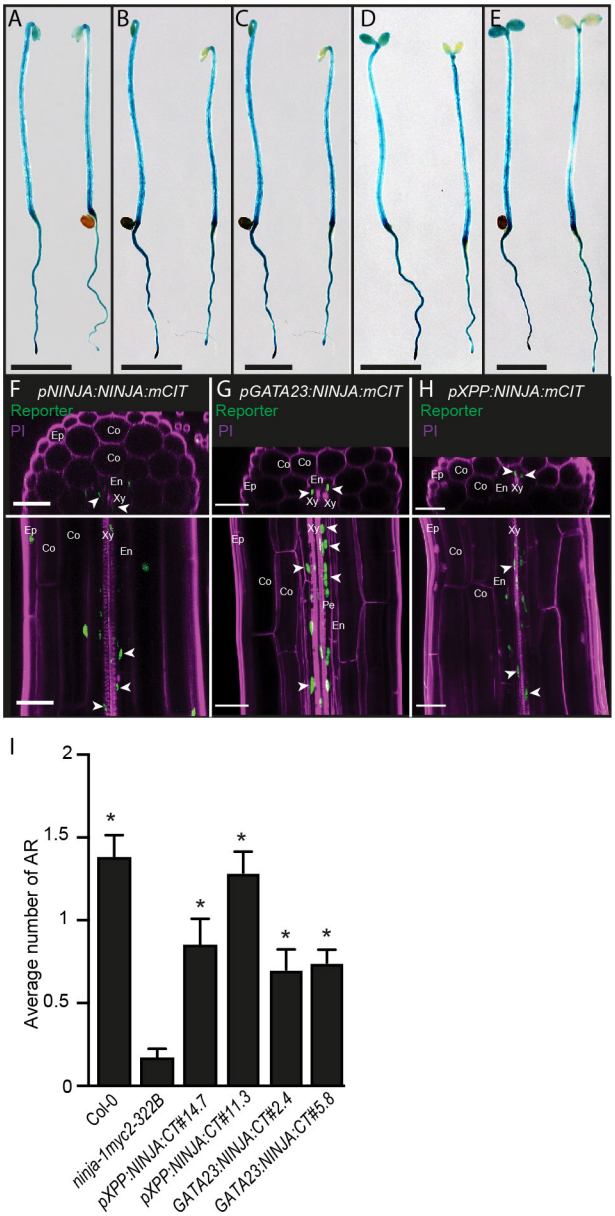

Figure 3: NINJA-dependent JA signaling inhibit ARI in pericycle cells.

(A) to (E) Spatiotemporal activity patterns of the *NINJA* and *MYC2* promoters, left and right, respectively in each panel. Seedlings expressing the *pNINJA:GUSplus* or *pMYC2:GUSplus* constructs were grown in the dark until their hypocotyls were 6-7 mm long (T0) (A) then either kept in the dark for 9 h (T9D)(B) and 24 h (T24D)(C) or transferred to the light for 9 h (T9L)(D) or 24 h (T24L)(E). Scale bars represent 6 mm.

(F) to (H) Representative images of etiolated hypocotyls expressing *pNINJA:NINJA:mCITRINE* (F), *pGATA23:NINJA:mCITRINE* (G), and *pXPP:NINJA:mCITRINE* (H) of seedlings grown in darkness until their hypocotyls were 6-7 mm long. The cell walls were counterstained magenta with propidium iodide (PI). Orthogonal

1031 views from epidermis to vasculature are shown in the top panels. Z-projections of the hypocotyl
1032 volume around the vasculature are shown in the bottom panels. The following cell types can be
1033 distinguished: Epidermis (Ep), Cortex (Co), Endodermis (En), Pericycle (Pe) and Xylem (Xy).
1034 In orthogonal views, the two protoxylem elements allow deduction of the direction of the xylem
1035 axis and thus the position of the xylem-pole pericycle. Arrowheads indicate signals in xylem-
1036 pole pericycle cells in green.
1037 (I) Average numbers of ARs produced by the *ninja-1myc2-322B* double mutant, two
1038 independent transgenic lines expressing *pXPP:NINJA:mCITRINE/ninja-1myc2-322B* or
1039 *pGATA23:NINJA:mCITRINE/ninja-1myc2-322B* and wild-type (Col-0) seedlings. A non-
1040 parametric Kruskal-Wallis test followed by Dunn's multiple comparison post-test indicated that
1041 *pXPP:NINJA:mCITRINE/ninja-1myc2-322B* (#14.7 and #11.3) and
1042 *pGATA23:NINJA:mCITRINE/ninja-1myc2-322B* (#2.4 and #5.8) produced significantly more
1043 ARs than the *ninja1myc2-322B* double mutant. Error bars indicate ± SEM ($n \geq 30$; $P < 0.006$).
1044

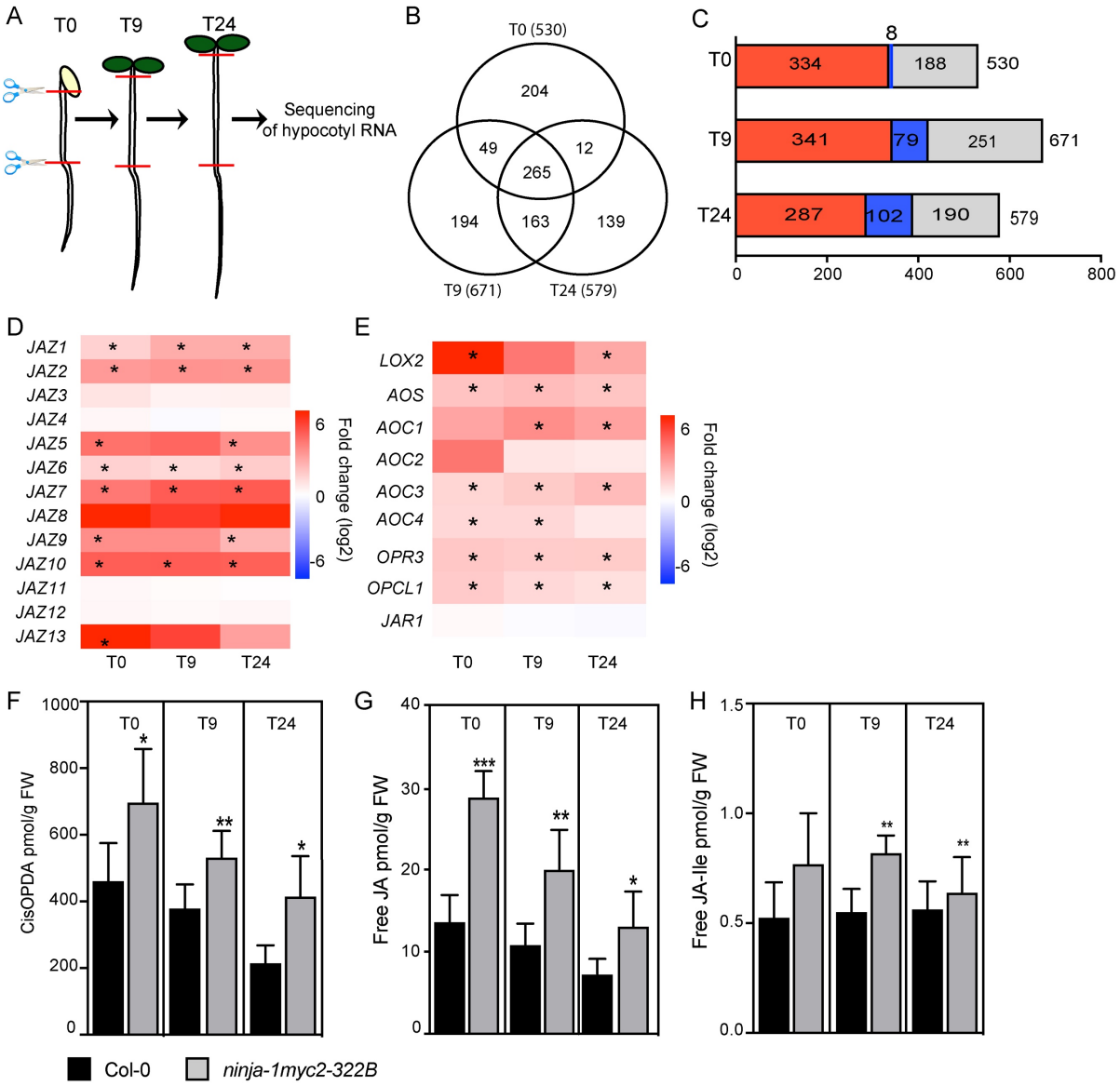

Figure 4: RNA-Seq revealed several DEGs between the *ninja-1myc2-322B* double mutant and wild-type seedlings.

(A) Schematic representation of the RNA-Seq experiment. Total RNA was extracted from hypocotyls of *ninja-1myc2-322B* double mutant and wild-type seedlings grown in the dark until their hypocotyls were 6-7 mm long (T0), and after their transfer to the light for 9 h (T9) or 24 h (T24).

(B) Venn diagram summarizing the DEGs between *ninja-1myc2-322B* double mutant and wild-type seedlings. (C) Enrichment of G-box (CACGTG, CACATG) or G-box-like (AACGTG, CATGTG CACGCG or CACGAG) motifs in the DEGs. Colors indicate upregulated genes (red) or downregulated genes (blue) containing at least one of the motifs. The gray color indicates the remaining DEGs, containing none of the mentioned motifs.

1057 (D) Heatmap of expression of the 13 *JAZ* genes. The map is based on fold-differences (log_2) in
1058 transcript abundance (based on RNA-Seq data) in *ninja-1myc2-322B* double mutant samples
1059 relative to the abundance in wild-type samples. Colors indicate upregulated genes (red) and
1060 downregulated genes (blue) in *ninja-1myc2-322B* double mutant relative to expression levels
1061 in wild-type seedlings. Values marked with asterisks are statistically significant.
1062 (E) Heatmap of expression selected JA biosynthesis genes. The map is based on fold-
1063 differences (log_2) in transcript abundance (based on RNA-Seq data) in *ninja-1myc2-322B*
1064 double mutant samples relative to the abundance in wild-type samples. Colors indicate
1065 upregulated genes (red) and downregulated genes (blue) in *ninja-1myc2-322B* relative to wild-
1066 type expression levels. Values marked with asterisks are statistically significant.
1067 (F) to (H) Endogenous jasmonate contents. (F) *cis*-OPDA, (G) free JA and (H) JA-Ile contents
1068 of hypocotyls of *ninja-1myc2-322B* and wild-type seedlings grown in the dark until their
1069 hypocotyls were 6 mm long (T0) and after their transfer to the light for 9 h (T9) and 24 h (T24).
1070 Asterisks indicate statistically significant differences between the mutant lines and wild-type
1071 plants according to ANOVA analysis (*, **, and *** indicate p values of $0.05 > p > 0.01$, 0.01
1072 $> p > 0.001$, and $p < 0.001$, respectively). Error bars indicate ± SD of six biological replicates.
1073

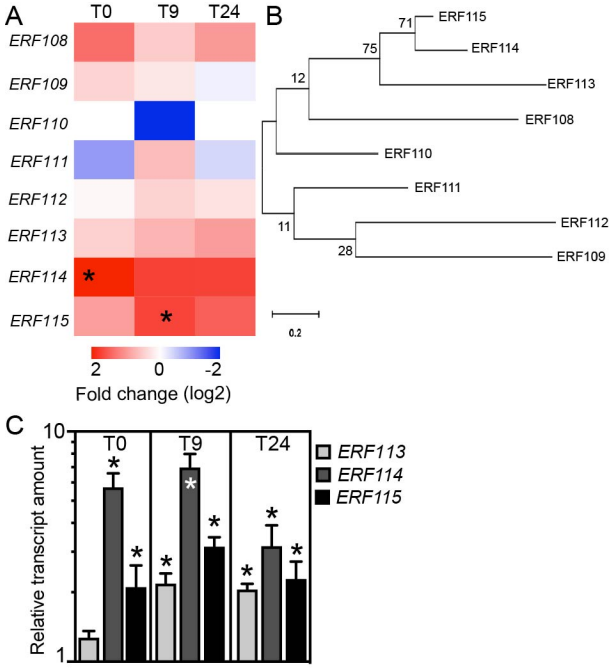

Figure 5: *ERF113*, *ERF114* and *ERF115* are induced by JA signaling.

(A) Heatmap of expression of the subgroup X *ERF family* members. The map is based on fold-differences ($\log_2$) in transcript abundance (based on RNA-Seq data) in *ninja-1myc2-322B* double mutant samples relative to the abundance in wild-type samples. Colors indicate upregulated genes (red) or downregulated genes (blue) in *ninja-1myc2-322B* relative to wild type expression levels. Values marked with asterisks are statistically significant.

(B) Phylogenetic tree of subgroup X of the AP2/ERF protein family derived from protein sequence alignment by the maximum likelihood method using MEGA X software (Kumar et al., 2018).

(C) Validation by qRT-PCR of mutation-induced shifts in *ERF113*, *ERF114* and *ERF115* expression profiles in the *ninja-1myc2-322B* double mutant (abundance of transcripts, in log10 scale, at indicated time points relative to their abundance in wild-type seedlings, which was arbitrarily set to 1). Error bars indicate ±SE obtained from three independent technical replicates. Asterisks mark significance differences between the genotypes according to a *t*-test

1108 ($P < 0.001$, $n = 3$). The experiment was repeated twice with independent biological replicates
1109 and gave similar results.
1110

1111

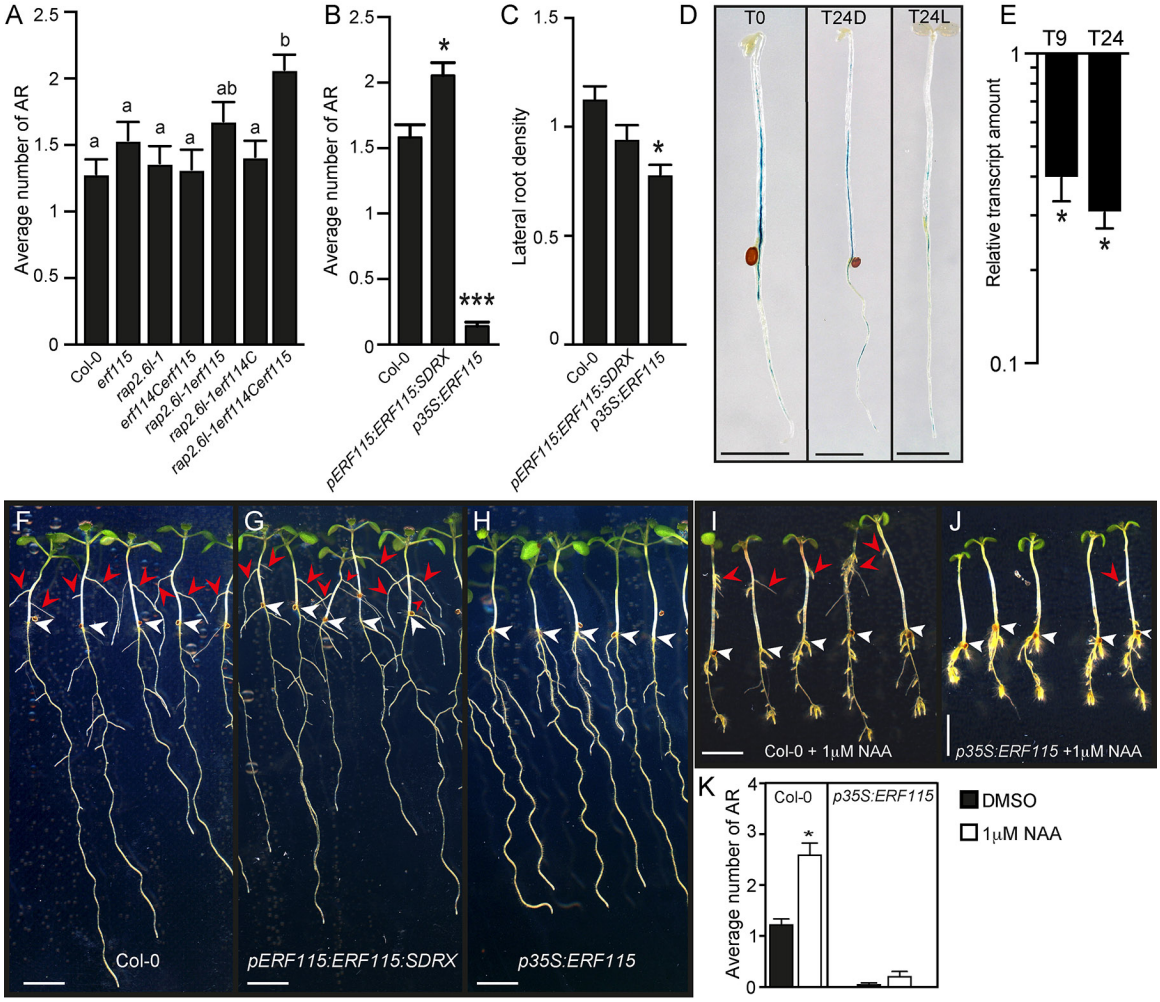

1112

1113

1114 **Figure 6: The *ERF115* gene is an inhibitor of ARI.**

1115 (A) Average numbers of AR produced by *erf* mutants and wild-type seedlings. One-way
1116 ANOVA combined with Tukey's multiple comparison post-test indicated that only the triple
1117 mutant *rap2-6lerf114Cerf115* significantly differed in this respect from wild-type (Col-0)
1118 plants. Error bars indicate ± SEM ($n \geq 40$, $P < 0.001$).

1119 (B) Average numbers of ARs produced by *35S:ERF115* and *pERF115:ERF115:SRDX* relative
1120 to numbers produced by wild-type plants. Data from two independent biological replicates,
1121 each of at least 40 seedlings, were pooled and averaged. A non-parametric Kruskal-Wallis test
1122 followed by Dunn's multiple comparison test indicated that numbers of ARs produced by the
1123 transgenic and wild-type plants significantly differed. Error bars indicate ± SEM ($n \geq 40$, $P <$
1124 0.02).

1125 (C) LR density of *35S:ERF115* and *pERF115:ERF115:SRDX* lines and wild type plants in AR
1126 phenotyping conditions. *35S:ERF115* mutants had significantly lower LR density than wild-
1127 type plants according to one-way ANOVA followed by Tukey's multiple comparison test.
1128 (D) Spatiotemporal activity pattern of the *ERF115* promoter, as shown by seedlings expressing
1129 the *pERF115:GUS* construct grown in the dark until their hypocotyls were 6-7 mm long (T0),
1130 and 24 h (T24L) after either transfer to the light or further growth in the dark (T24D). Scale
1131 bars represent 6 mm.
1132 (E) Validation by qRT-PCR of *ERF115* expression patterns in wild-type plants. Presented gene
1133 expression values are relative (in log10 scale) to the expression at T0, for which the value was
1134 arbitrarily set to 1. Error bars indicate ±SE obtained from three independent technical replicates.
1135 A *t*-test indicated that values indicated by an Asterisks indicate values that significantly differ
1136 from the T0 values ($P < 0.001$, $n = 3$). The experiment was repeated twice with independent
1137 biological replicates and gave similar results.
1138 (F) to (H) Representative photos of (F) wild-type, (G) *35S:ERF115*, and (H)
1139 *pERF115:ERF115:SRDX* seedlings.
1140 (I) to (J) Representative photos of wild-type and *35S:ERF115* seedlings grown in the dark until
1141 their hypocotyls were 6-7 mm long, then transferred to fresh medium containing either mock
1142 solution or 1 μM naphthaleneacetic acid (NAA) for seven more days under long-day conditions
1143 to induce ARs. Arrowheads indicate hypocotyl-root junctions (white) or ARs (red). Scale bars
1144 represent 6 mm.
1145 (K) Average numbers of ARs produced by wild-type and *35S:ERF115* plants in response to
1146 NAA. Wild-type seedlings produced significantly more ARs after NAA treatment than after
1147 mock-treatment according to a Mann-Whitney test ($n \geq 40$, $P < 0.0001$), but NAA treatment
1148 had no significant effect on AR production by *35S:ERF115* plants. Error bars indicate ± SEM.
1149

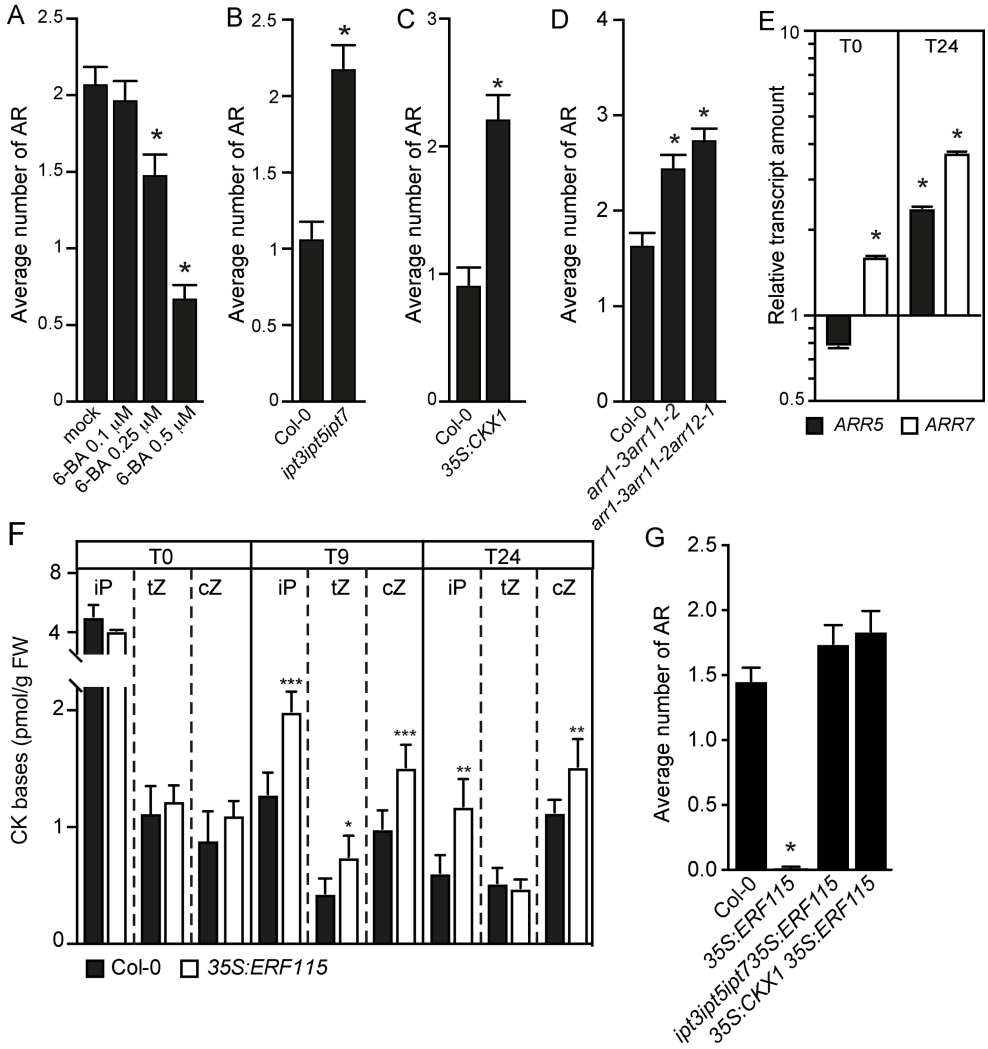

Figure 7: Cytokinins inhibit ARI downstream of *ERF115*.

1183 (A) Average numbers of ARs produced by wild-type (Col-0) seedlings, which were grown in
1184 the dark until their hypocotyls were 6-7 mm long, then transferred to fresh medium containing
1185 either mock solution or solutions with indicated concentrations of 6-Benzylaminopurine (6-
1186 BA). The seedlings were kept for seven more days under long-day conditions to induce ARs.
1187 Seedlings treated with 0.25 μM or 0.5 μM 6-BA significantly differed from the mock-treated
1188 controls, according to a non-parametric Kruskal-Wallis test followed by Dunn's multiple
1189 comparison test. Error bars indicate ± SEM ($n \geq 40$, $P < 0.004$).
1190 (B) to (D) Average numbers of ARs produced by wild-type plants and: (B) *ipt3ipt5ipt7* triple
1191 mutants defective in CK biosynthesis, (C) *35S:CKX1 CYTOKININ OXIDASE1*-overexpressing
1192 plants, which have reduced CK contents due to increased rates of degradation, and (D) CK
1193 signaling mutants.
1194 (E) Relative amounts of *ARR5* and *ARR7* transcripts quantified by qRT-PCR. Total RNA was
1195 extracted from hypocotyls of *35S:ERF115* and the wild-type seedlings grown in AR-inducing
1196 conditions, as outlined above, at T0 (at the end of the dark incubation) and T24 (24 hours later).
1197 The gene expression values are relative to wild-type values, which were arbitrarily set to 1. The
1198 Y axis scale is a $\log_{10}$ scale. Error bars indicate ± SEM obtained from three technical replicates.
1199 Asterisks indicate values that significantly differ from wild-type values according to a *t*-test (P
1200 < 0.001, $n = 3$). The experiment was repeated once with an independent biological replicate and
1201 gave similar results.
1202 (F) Endogenous contents of active CK bases. The CK bases were quantified in the hypocotyls
1203 of *35S:ERF115* and the wild-type seedlings grown in the dark until they were 6-7 mm long
1204 (T0) and after their transfer to the light for 9 h (T9) or 24 h (T24). Asterisks indicate statistically
1205 significant differences between mutant and wild-type plants according to ANOVA (*, **, and
1206 *** indicate P-values of $0.05 > P > 0.01$, $0.01 > P > 0.001$, and $P < 0.001$, respectively). Error
1207 bars indicate ± SD of six biological replicates.
1208 (G) Average numbers of ARs produced by *35S:ERF115* plants, *35S:ERF115* plants
1209 overexpressing *CKX1* from a *35S:CKX1* construct and the *ipt3,5,7* triple mutant overexpressing
1210 *ERF115* from a *35S:ERF115* construct. Numbers produced by the multiple mutants
1211 significantly differed from numbers produced by *35S:ERF115* plants according to a non-
1212 parametric Kruskal-Wallis test followed by Dunn's multiple comparison test. Error bars
1213 indicate ± SEM ($n \geq 40$, $P < 0.0001$).
1214